Atmos. Chem. Phys. Discuss., doi:10.5194/acp-2016-1089, 2017
Manuscript under review for journal Atmos. Chem. Phys.
Published: 4 January 2017

Atmospheric Chemistry and Physics Discussions

Higher measured than modeled ozone production at increased NO_x levels in the Colorado Front Range

Bianca Baier[1,a,*], William Brune[1], David Miller[1], Donald Blake[2], Russell Long[3], Armin Wisthaler[4,5], Christopher Cantrell[6], Alan Fried[7], Brian Heikes[8], Steven Brown[9,10], Erin McDuffie[9,10,11], Frank Flocke[12], Eric Apel[12], Lisa Kaser[12], and Andrew Weinheimer[12]

[1]Department of Meteorology and Atmospheric Science, The Pennsylvania State University, University Park, PA, USA
[2]School of Physical Sciences, University of California, Irvine, CA, USA
[3]US EPA National Exposure Research Lab, Research Triangle Park, NC, USA
[4]Institute of Ion Physics and Applied Physics, University of Innsbruck, Austria
[5]Department of Chemistry, University of Oslo, Norway
[6]Department of Atmospheric and Oceanic Sciences, University of Colorado Boulder, Boulder, CO, USA
[7]INSTAAR, University of Colorado Boulder, Boulder, CO, USA
[8]Graduate School of Oceanography, The University of Rhode Island, Kingston, RI, USA
[9]Chemical Sciences Division, NOAA Earth System Research Laboratory, Boulder, CO, USA
[10]Department of Chemistry and Biochemistry, University of Colorado Boulder, Boulder, CO, USA
[11]Cooperative Institute for Research in the Environmental Sciences, University of Colorado Boulder, Boulder, CO, USA
[12]Atmospheric Chemistry Observations and Modeling Laboratory, National Center for Atmospheric Research, Boulder, CO, USA
[a]now at: Cooperative Institute for Research in the Environmental Sciences, University of Colorado Boulder, Boulder, CO, USA and Global Monitoring Division, NOAA Earth System Research Laboratory, Boulder, CO, USA

Correspondence to: Bianca Baier (bianca.baier@noaa.gov)

Abstract. Chemical models must accurately calculate the ozone formation rate, $P(O_3)$, to accurately predict ozone levels and test mitigation strategies. However, model chemical mechanisms can contain large uncertainties in $P(O_3)$ calculations, which can create uncertainties in ozone forecasts especially during the summertime when $P(O_3)$ can be high. One way to test mechanisms is to evaluate model $P(O_3)$ using direct measurements. During summer 2014, the Measurement of Ozone Production Sensor (MOPS) measured net $P(O_3)$ in Golden, CO, approximately 25 km west of Denver along the Colorado Front Range. Net $P(O_3)$ was compared to rates calculated by a photochemical box model using a lumped and a more explicit chemical mechanism. Observed $P(O_3)$ was up to a factor of two higher than that modeled during early morning hours when nitric oxide (NO) levels were high, contrary to traditional ozone chemistry theory. This disagreement may be due to model underestimation of hydroperoxyl (HO_2) radicals relative to observations at high NO levels. These additional peroxyl radicals could come from the MOPS chamber chemistry or from missing volatile organic compounds co-emitted with NO_x; additional cycling of OH into HO_2 through reactions involving nitric oxide provides an alternate explanation for higher measured than modeled $P(O_3)$. Although the MOPS measurements are new, comparisons of observed and modeled $P(O_3)$ in NO space show a similar behavior to other comparisons between $P(O_3)$ derived from measurements and modeled $P(O_3)$. These comparisons can have implications for the sensitivity of $P(O_3)$ to nitrogen oxides and volatile organic compounds during morning hours, and

Atmos. Chem. Phys. Discuss., doi:10.5194/acp-2016-1089, 2017
Manuscript under review for journal Atmos. Chem. Phys.
Published: 4 January 2017

Atmospheric Chemistry and Physics Discussions

can possibly affect ozone reduction strategies for the region surrounding Golden, CO in addition to other urban and suburban areas that are in non-attainment with national ozone regulations.

1 Introduction

Ground-level ozone (O_3) is a hazardous air pollutant abundant in cities and their surrounding areas. Awareness of its detrimental health effects on both humans and plants has led to the Clean Air Act of 1970 and the development of National Ambient Air Quality Standards (NAAQS) (Krupa and Manning, 1988; Bell et al., 2004; US EPA, 2013, 2016b). These standards have been successful in reducing O_3 by approximately 32% in the United States since 1980. However, current O_3 levels are stabilizing and even increasing again in the western United States (US EPA, 2016a). Understanding why these trends are occurring in areas despite more stringent emissions controls is crucial for further reduction of O_3 levels within the United States.

Boundary layer O_3 levels are dependent upon both chemical and meteorological processes described in the following equation:

$$\frac{\partial[O_3]}{\partial t} = P(O_3) + \frac{w_e \triangle O_3 - u_d[O_3]}{H} - \nabla \cdot (\mathbf{v}[O_3]), \quad (1)$$

where $\partial[O_3]/\partial t$ is the local O_3 time rate of change, $P(O_3)$ is the instantaneous net photochemical O_3 production rate, $(w_e \triangle O_3 - u_d[O_3])/H$ is the combined entrainment and deposition rate of O_3 in or out of the mixing layer of height H, and $\nabla \cdot (\mathbf{v}[O_3])$ is the O_3 advection rate. All of the physics, chemistry, and meteorology needed to solve this equation are included in chemical transport models (CTMs), which are used to design and test reduction strategies. For areas where local production is the dominant source of O_3, the term in Eq. (1) that will reduce O_3 through local emissions control strategies is $P(O_3)$. Thus, understanding and accurately calculating O_3 formation is crucial for its mitigation.

Ozone formation chemistry has been well-documented for decades (Haagen-Smit et al., 1953; Finlayson-Pitts and Pitts, 1977; Seinfeld and Pandis, 2012; Calvert et al., 2015). The oxidation of volatile organic compounds (VOCs) by the hydroxyl radical (OH) produces hydroperoxyl (HO_2) and organic peroxyl (RO_2) radicals. These peroxyl radicals react with nitrogen oxide (NO) to form nitrogen dioxide (NO_2), which is photolyzed to form new O_3 outside of the NO_x photostationary state (PSS): a steady-state reaction sequence involving NO_x (NO_2 + NO) and O_3. Thus, chemical O_3 production occurs through reactions with NO and peroxyl radicals described in Eq. (2), where k denotes a bimolecular reaction rate coefficient. Equation (3) describes the chemical O_3 (or NO_2) destruction rate or rate of removal to reservoir species as the fraction of $O(^1D)$ molecules resulting from O_3 photolysis that react with H_2O to form OH; reactions of O_3 with HO_x (HO_2 + OH); the production of organic nitrates [$P(RONO_2)$], including the net production of peroxyacyl nitrates; and O_3 loss through reactions with

Atmos. Chem. Phys. Discuss., doi:10.5194/acp-2016-1089, 2017
Manuscript under review for journal Atmos. Chem. Phys.
Published: 4 January 2017

Atmospheric Chemistry and Physics Discussions

alkenes and halogens. The net instantaneous O_3 production rate, $P(O_3)$, is then defined as the difference between O_3 chemical production and loss rates in Eq. (4) (Baier et al., 2015):

$$P_{chem} = k_{NO+HO_2}[NO][HO_2] + \sum_{i=1}^{N} k_{NO+RO_{2i}}[NO][RO_2]_i \quad (2)$$

$$L_{chem} = J_{O_3} f_{H_2O}[O_3] + k_{OH+O_3}[OH][O_3] + k_{HO_2+O_3}[HO_2][O_3] + P(RONO_2) + k_{OH+NO_2}[OH][NO_2] + L(O_3)_{alkenes} + L(O_3)_{halogens} \quad (3)$$

$$P(O_3) = P_{chem} - L_{chem}. \quad (4)$$

Equations (2) and (3) illustrate the non-linear dependence of $P(O_3)$ on both NO_x and the production of HO_x from VOC oxidation. That is, these chemical species are involved in both the production and destruction of O_3 molecules. Increases in NO can cause $P(O_3)$ to initially increase until NO_x levels are sufficiently high to react with OH, thereby removing HO_x and NO_x from the reaction system and decreasing $P(O_3)$. Therefore, $P(O_3)$ is largely dependent upon the cycling between HO_x and NO_x in the atmosphere; the exact NO_x level at which this crossover occurs is sensitive to the production rate of HO_x radicals (Jaegle et al., 1998; Trainer et al., 2000; Thornton et al., 2002; Ren et al., 2005). In a NO_x-sensitive regime, $P(O_3)$ varies with the square root of $P(HO_x)$ and decreases in NO_x are more effective in decreasing O_3 than decreases in VOCs. Conversely, in a VOC-sensitive regime, $P(O_3)$ varies linearly with $P(HO_x)$ and decreases in VOCs are more effective in decreasing O_3, while further NO_x decreases can act to increase O_3 (Kleinman et al., 1997; Seinfeld and Pandis, 2012). If the sensitivity of $P(O_3)$ to NO_x and VOCs is known, efficient O_3 mitigation strategies can be devised that target precursor emissions and more effectively reduce O_3 in polluted regions.

The gas-phase chemical mechanisms used in CTMs rely on a number of model input parameters to calculate $P(O_3)$ such as measurements of inorganic and organic chemical species; temperature- and pressure-dependent reaction rates; photolysis frequencies; and product yields of reactions. As the chemical processes contributing to O_3 formation are both vast and complex, it is difficult to portray atmospheric reactions in their entirety. Thus, mechanisms are simplified to describe the complex chemical state of the atmosphere. While inorganic chemistry is generally similar between reduced and more explicit mechanisms, differences in VOC aggregation schemes can create variance in modeled $P(O_3)$, O_3, or other important O_3 precursor predictions (Jeffries and Tonnesen, 1994; Olson et al., 1997; Kuhn et al., 1998; Luecken et al., 1999; Dodge, 2000; Tonnesen and Dennis, 2000; Jimenez et al., 2003; Luecken et al., 2008; Chen et al., 2010).

The traditional view of O_3 production chemistry is not consistent with all observations. First, numerous studies have shown that both zero-dimensional and three-dimensional modeled HO_2 – or the HO_2 to OH ratio – is underestimated at values of NO

Atmos. Chem. Phys. Discuss., doi:10.5194/acp-2016-1089, 2017
Manuscript under review for journal Atmos. Chem. Phys.
Published: 4 January 2017

Atmospheric Chemistry and Physics Discussions

greater than a few parts per billion by volume (ppbv) (Faloona et al., 2000; Martinez et al., 2003; Ren et al., 2003; Emmerson et al., 2005; Shirley et al., 2006; Emmerson et al., 2007; Kanaya et al., 2007, 2008; Dusanter et al., 2009; Chen et al., 2010; Sheehy et al., 2010; Ren et al., 2013; Czader et al., 2013; Brune et al., 2015), although this underestimation was less severe and only evidenced above 20 ppbv in some studies due to significant VOC reactivity (Shirley et al., 2006). Nonetheless, $P(O_3)$ calculated from measured HO_2 radicals can routinely be more than double the $P(O_3)$ calculated from modeled HO_2 (Kanaya et al., 2008; Ren et al., 2013; Brune et al., 2015). Second, Im et al. (2015) and Appel et al. (2007) found that CTMs typically underestimate O_3 levels above 60-80 ppbv and overestimate O_3 below 30 ppbv: errors that are typically accredited to emissions and chemical mechanism choice. Summertime O_3 predictions were most sensitive to regional production due to increased photochemical activity rather than transport (Im et al., 2015). Finally, studies in the northeastern United States have shown that CTMs underestimate the effects of NO_x emissions reductions on O_3 (Gilliland et al., 2008). Thus, chemical mechanism uncertainties can greatly affect O_3 predictions and even reverse the order of O_3 production sensitivity to its precursors, decreasing confidence in models used for developing emissions reduction strategies.

The Measurement of Ozone Production Sensor (MOPS) directly measures $P(O_3)$ and can help to evaluate O_3 formation calculated from chemical mechanisms (Cazorla and Brune, 2010; Baier et al., 2015). Cazorla et al. (2012) compared direct O_3 production rates to both modeled $P(O_3)$ and that calculated from measured peroxyl radicals. Afternoon production rates were statistically similar between observed, calculated, and modeled $P(O_3)$. In the early morning, MOPS $P(O_3)$ magnitudes were similar to those calculated from measured radical species, but were almost twice as large as modeled rates. Similarly, observed $P(O_3)$ and that calculated from HO_2 observations were approximately equal to that modeled for NO levels up to 1 ppbv, but were significantly larger for higher values of NO (Ren et al., 2003; Spencer et al., 2009; Ren et al., 2013; Cazorla et al., 2012; Brune et al., 2015).

$P(O_3)$ was measured in Golden, CO in Summer 2014 during the Deriving Information on Surface conditions from COlumn and VErtically-resolved observations Relevant to Air Quality (DISCOVER-AQ) field campaign and the Front Range Air Pollution and Photochemistry Experiment (FRAPPÈ). This paper describes comparisons between $P(O_3)$ measured *in situ* by a second-generation MOPS and modeled $P(O_3)$ using both lumped and near-explicit chemical mechanisms. Finally, we examine possible causes for differences observed between measured and modeled $P(O_3)$.

2 Methods

2.1 MOPS measurements

A second-generation MOPS directly measures the instantaneous O_3 production rate, $P(O_3)$, with an improved chamber and airflow design. The method is briefly described here; a more thorough technical description of the MOPS and its modifications is detailed in Baier et al. (2015). The second-generation design aims to decrease artificial chemistry induced by air-surface interactions within the chambers. The difference in O_x (O_3 + NO_2) is continuously sampled by two 26.9-L trapezoidal environmental chambers with airflow somewhat like a sheath flow to isolate sampled air from chamber surfaces. A sample chamber is transparent and undergoes the same O_3 photochemistry as the atmosphere, while a reference chamber is covered with a film

Atmos. Chem. Phys. Discuss., doi:10.5194/acp-2016-1089, 2017
Manuscript under review for journal Atmos. Chem. Phys.
Published: 4 January 2017

Atmospheric Chemistry and Physics Discussions

that blocks all ultraviolet (UV) radiation of wavelengths below 400 nm, suppressing the radical chemistry essential for new O_3 production. Positioned after the chambers, a highly-efficient UV light-emitting diode photolyzes NO_2 into O_3 in air coming through separate tubing from both the sample and reference chambers. This converter cancels any differences in the NO_x PSS caused by the reference chamber film. The difference in O_x divided by the exposure time of air in the MOPS chambers yields the net O_3 production rate as $P(O_x)$.

The MOPS absolute uncertainty (1σ) is $\pm$ 11 ppbv h^{-1} for 10-min measurements (Baier et al., 2015). At times, the MOPS measures artificial positive and negative O_3 production rates. Like previous discussion in Cazorla et al. (2012), negative $P(O_3)$ rates are unrealistic during the day when OH production is large enough to sustain new NO_2 and subsequent O_3 formation from VOC oxidation. Anomalous positive $P(O_3)$ is sometimes measured before sunrise or in the early morning, also indicating possible artifacts in the MOPS measurements.

MOPS chamber loss tests and flow visualizations have indicated that wall loss of O_x is negligible (Cazorla and Brune, 2010; Baier et al., 2015). Although the MOPS precision is typically 5 ppbv h^{-1} (1σ), O_3 analyzer drifting can degrade this precision. Random, non-linear analyzer drifting occurs during the day and, like previous studies, is hypothesized to stem from humidity differences between the UV absorption cells in the MOPS Thermo Scientific O_3 analyzer (US EPA, 1999; Wilson and Birks, 2006; Baier et al., 2015). Drifting is partially corrected through zeroing the MOPS chambers either by removing the reference chamber film for an entire day or by measuring $P(O_3)$ on cooler, cloudy days when O_3 formation is likely near zero (Baier et al., 2015). Since the same O_3 formation will occur in both chambers on these occasions, this method should retrieve a "zero" $P(O_3)$ time series that can be subtracted off of the MOPS raw data. However, this zero only partially corrects for this drifting due to varying humidity from day to day. Consequently, the corrected MOPS baseline routinely drifts between -5 and 5 ppbv hr^{-1} most mornings and late afternoons when $P(O_3)$ is typically low.

The MOPS chamber "sheath" airflow deters species adsorption (desorption) to (from) surfaces with high flow rates of approximately 20 LPM along the walls of the chambers (Baier et al., 2015). Air is then sampled from a slower, center flow that is isolated from the chamber walls. It is known that NO_2 adsorption onto the chamber walls can result in the heterogeneous formation of nitrous acid (HONO) through the reaction of NO_2 with water vapor adsorbed onto surfaces (Finlayson-Pitts et al., 2003). A photolytic HONO source has also been previously reported (Rohrer et al., 2005; George et al., 2005; Stemmler et al., 2006; Langridge et al., 2009; Lee et al., 2016; Crilley et al., 2016). During the 2013 DISCOVER-AQ study in Houston, TX, some excess HONO was measured in the MOPS chambers, which can create excess OH and O_3 production. This HONO source has been found to be correlated with relative humidity, temperature, and J_{NO_2}, and actions were taken prior to DISCOVER-AQ 2014 to reduce this measurement bias by approximately 30%. We calculate that this artifact reflects a maximum 3.5-7 ppbv h^{-1} positive bias in observed $P(O_3)$ for this study. The bias and random errors are incorporated into a propagation of uncertainty analysis in order to calculate the MOPS absolute uncertainty (Baier et al., 2015).

2.2 Site description and ancillary measurements

Second-generation MOPS measurements were recorded for 19 days in Golden, CO (39^{o}44.623'N, 105^{o}10.679'W), which is located approximately 25 km west of the Denver metropolitan area. Commerce City, which houses several oil refineries, is

Atmos. Chem. Phys. Discuss., doi:10.5194/acp-2016-1089, 2017
Manuscript under review for journal Atmos. Chem. Phys.
Published: 4 January 2017

Atmospheric Chemistry and Physics Discussions

located 30 km to the northeast. The Golden measurement site lies east of the Front Range, atop the South Table Mountain mesa (1833 m asl) and amidst grass-covered terrain. The Colorado summertime climate is hot and arid with intense solar radiation. These meteorological conditions can be conducive for high O_3 formation from both local and advected precursor emissions. Ozone production can also be affected by diurnally varying, thermally driven winds; morning heating of mountains invokes easterly upslope flow, transporting precursors from Denver and the urban corridor of the Front Range westward, while downsloping afternoon westerlies can re-circulate these pollutants eastward to lower elevations (Banta, 1984).

Measurements used to constrain the models in this study were obtained on ground-based and aircraft platforms during DISCOVER-AQ and FRAPPÈ. Both studies were co-located in the Colorado Front Range between 17 July and 10 August 2014. Continuous, ground-based 1-min measurements of meteorological parameters and inorganic chemical species include temperature, pressure, and relative humidity, O_3, sulfur dioxide, and NO_x. In the absence of continuous ground-based VOC measurements, C_2-C_{10} non-methane hydrocarbons (NMHC) and organic nitrates were measured from 72 total whole-air canister (WAC) samples that were collected in Golden and analyzed by gas chromatography (GC) and gas chromatography-mass spectrometry (GC-MS) in the laboratory. A daily average of five samples were taken over 16 days, with heavier sampling between 0700 and 1200 local time (LT) to capture VOC mixing ratios during morning O_3 production hours, and sparser sampling in the afternoon between 1400 and 1800 LT to examine advection from areas east of Golden, CO such as the Denver metropolitan region and the Commerce City region. Median diurnal values of VOCs were constructed from these point measurements to provide constraints for the model calculations. In addition, we initialized backward Hybrid Single-Particle Lagrangian Integrated Trajectory (HYSPLIT) models at 300 and 500 m heights beginning at 1600 LT and run for 12 hours using North American Model (NAM) meteorological data to determine whether the airflow in Golden could have originated from these eastern regions (Stein et al., 2015; Rolph, 2016). In general, higher NO_x and anthropogenic VOC mixing ratios were measured when HYSPLIT indicated flow from eastern pollution sources. For days when measurements were made in these plumes, separate median diurnal VOC values were constructed to more accurately represent the VOC speciation observed in Golden.

Canister VOCs were supplemented by boundary layer inorganic and organic chemical species measurements obtained on the NASA P-3B and NSF/NCAR C-130 aircraft and constant, median values were calculated for times when the aircraft were in the vicinity of Golden and used in the model (Table 1, Table S1). Measurements aboard the P-3B were used when it was directly overhead of Golden, CO, while C-130 measurements were used when this aircraft was within roughly 20 km of the measurement site. More information on the DISCOVER-AQ and FRAPPÈ campaigns, aircraft and ground-based platforms, and measurement methods can be found at http://www-air.larc.nasa.gov/missions/discover-aq/discover-aq.html and https://www2.acom.ucar.edu/frappe.

2.3 Model description

Two types of chemical mechanisms were used in zero-dimensional photochemical box models to calculate $P(O_3)$ for the entire DISCOVER-AQ and FRAPPÉ campaign period. We used the lumped Regional Atmospheric Chemistry Mechanism version 2 (RACM2) (Stockwell et al., 1997; Goliff et al., 2013), and the near-explicit Master Chemical Mechanism version 3.3.1 (MCMv331) (Jenkin et al., 2003; Bloss et al., 2005; Jenkin et al., 2015). An exhaustive list of model constraints is displayed in

Atmos. Chem. Phys. Discuss., doi:10.5194/acp-2016-1089, 2017
Manuscript under review for journal Atmos. Chem. Phys.
Published: 4 January 2017

Atmospheric Chemistry and Physics Discussions

Table 1. Cloud-free photolysis rates were calculated using the Tropospheric Ultraviolet (TUV) model (Madronich and Flocke, 1999) for Golden, CO. These photolysis rates were scaled to J_{NO_2} calculated from continuous pyranometer measurements (LI-COR, LI-200 series) using the relationship described in Trebs et al. (2009) and used to constrain the models. All model constraints were interpolated to a 10-minute time step and input into the model to calculate $P(O_3)$ for the campaign period. The system of differential equations generated from both chemical mechanisms was integrated for 24 hours to allow reactive intermediates to reach steady-state. In addition, longer-lived inputs not constrained by the model were given a 24-hour lifetime to both prevent buildup of these species and to roughly account for advection or dilution losses. Modeled $P(O_3)$ is largely insensitive to this loss rate. We note that, although transport and entrainment processes can also influence O_3 levels, zero-dimensional model runs described here do not include these processes. Instead, we focus on net $P(O_3)$, which is calculated with Eqs. 2-4 using modeled output.

2.4 Model uncertainty assessment

2.4.1 RACM2

The RACM2 model includes 119 species and 363 reactions, and is run using the FACSIMILE solver (Stockwell et al., 1997; Goliff et al., 2013). An explicit isoprene chemistry scheme has replaced the original RACM2 isoprene chemistry, and is highlighted in Paulot et al. (2009) and Mao et al. (2013). As this mechanism aggregates VOCs based on their functional groups and OH reactivity, the RACM2 significantly reduces the number of model inputs and parameters over more explicit mechanisms that treat VOCs and their intermediate products separately.

Model uncertainty is traditionally evaluated through sensitivity analyses in order to identify inputs (observational data) and parameters (reaction rates and product yields) that create the most variance in a model output of interest. These inputs are hereby called “influential" inputs. The RACM2 model uncertainty is assessed through the use of a global sensitivity analysis for daylight hours between 0600 and 1800 LT.

A Random Sampling-High Dimensional Model Representation (RS-HDMR) analysis was performed, which varies hundreds of model constraints with relatively low computational expense (Rabitz and Alis, 1999; Li et al., 2006, 2010). The variance in modeled $P(O_3)$ due to changes in influential model constraints was calculated, with the $P(O_3)$ 1σ uncertainty derived as the total $P(O_3)$ standard deviation divided by its mean from time periods evaluated between 0600 and 1800 LT. The RS-HDMR technique used for the RACM2 model runs is detailed in Chen and Brune (2012) and Chen et al. (2012). An overview of model input uncertainties and a description of this global sensitivity analysis are presented in supplementary documentation.

2.4.2 MCMv331

The MCMv331 (Jenkin et al., 1997; Saunders et al., 2003; Bloss et al., 2005; Jenkin et al., 2015), is freely available at http://mcm.leeds.ac.uk/MCM and is run using a MATLAB framework described in Wolfe et al. (2011). This mechanism includes roughly 6,000 species and 17,000 reactions, treats VOCs and their intermediates separately, and uses explicit isoprene degradation chemistry described in Jenkin et al. (2015). Because of the large number of inputs in this near-explicit mechanism,

Atmos. Chem. Phys. Discuss., doi:10.5194/acp-2016-1089, 2017
Manuscript under review for journal Atmos. Chem. Phys.
Published: 4 January 2017

Atmospheric Chemistry and Physics Discussions

the MCMv331 uncertainty was assessed through a local sensitivity approach. That is, inputs were set to their upper and lower uncertainty limits in a one-at-a-time fashion while all other constraints were held at their original values. Total MCMv331 uncertainty was calculated by adding in quadrature the upper and lower percent deviations in $P(O_3)$ due to perturbations in model constraints relative to the MCMv331 base case. Input and parameter groups that were varied to derive this uncertainty are described in supplemental documentation.

3 Results

3.1 Campaign observations and $P(O_3)$ time series

Observed and modeled $P(O_3)$ were compared for 19 days between 17 July and 10 August 2014 in Golden (Fig. 1). From 17-27 July, the campaign was characterized by a warmer, drier period followed by a relatively cooler, wetter period until the end of the study. Daily O_3 mixing ratios typically peaked between 1300-1800 LT with a median value of 59 ppbv. Higher O_3 levels exceeding 80 ppbv were observed on 22, 28, and 29 July as well as 3 August. The highest O_3 levels were observed on 22 July with a maximum mixing ratio of approximately 90 ppbv.

Due to the terrain of the Front Range, the average diel wind direction during the campaign period was westerly before 0900 LT, easterly to northeasterly from 0900 to 1400 LT, and then westerly again after 1400 LT, with diel speeds ranging between 2-3.5 m s^{-1}. Thus, $P(O_3)$ in Golden can be influenced by pollutants advected from nearby eastern source regions during the mid-morning to early afternoon.

The MOPS $P(O_3)$ maxima were routinely higher than 10 ppbv h^{-1} on most measurement days, with diurnal peaks between 0900-1100 LT. Observed $P(O_3)$ maxima on individual days range from 10 ppbv h^{-1} to almost 40 ppbv h^{-1} (Fig. 1). Observed baseline $P(O_3)$ values were typically between -5 and 5 ppbv h^{-1}. However, the MOPS measured $P(O_3)$ less than -10 ppbv h^{-1} on some early mornings and late afternoons. These negative values are likely due to our inability to correct for O_3 analyzer drifting, which is exaggerated by high humidity or drastic changes in humidity during the measurement period. To account for possible anomalous $P(O_3)$ measurements due to humidity or its changes, MOPS data during these time periods have been removed from this analysis. Despite this artifact, MOPS variations were generally consistent with observed diurnal O_3 variations, with higher $P(O_3)$ measured on days where O_3 mixing ratios were greater than 70 ppbv (Fig. 1).

3.2 Modeled $P(O_3)$ time series and comparisons to measurements

Full-campaign modeled $P(O_3)$ is also shown in Fig. 1. Modeled $P(O_3)$ maxima were exhibited between 0900-1200 LT with values generally 10 ppbv h^{-1} or lower. The modeled $P(O_3)$ variations, however, were not always consistent with O_3 variations, with some of the highest $P(O_3)$ calculated for rather low O_3 days (20-21 July and 25 July). The RACM2 and MCMv331 $P(O_3)$ behavior was similar throughout the campaign period although occasionally, the MCMv331 $P(O_3)$ indicated spikes throughout the day where the RACM2 did not. This result is perhaps due to the more explicit treatment of VOCs and their intermediate

Atmos. Chem. Phys. Discuss., doi:10.5194/acp-2016-1089, 2017
Manuscript under review for journal Atmos. Chem. Phys.
Published: 4 January 2017

Atmospheric Chemistry and Physics Discussions

products in the MCMv331 versus the RACM2. Nonetheless, the RACM2 generally produces $P(O_3)$ patterns similar to that produced by the more explicit MCMv331.

In Fig. 2, median diel variations of MOPS and modeled $P(O_3)$ are shown for MOPS measurement days. Indicated by the 25th, median, and 75th percentiles, observed $P(O_3)$ began to increase around 0800 LT, was highest from 0900 to 1100 LT and then decreased later in the day. Modeled $P(O_3)$ generally followed the same diurnal pattern and was in rough agreement with the MOPS in the afternoon. Measured and modeled $P(O_3)$, however, were less similar during early morning peak $P(O_3)$ hours when NO_x and VOC levels were higher due to abundant local and advected rush hour traffic emissions. The majority of the MOPS $P(O_3)$ measurements exhibited maxima that are up to a factor of two higher than modeled $P(O_3)$ values during this time period.

Several reasons provide confidence in these $P(O_3)$ comparisons, which result in higher $P(O_3)$ than that modeled during the morning hours despite the MOPS absolute uncertainty. First, median $P(O_3)$ values were used instead of the mean to compare MOPS and modeled $P(O_3)$ so as not to bias diurnal $P(O_3)$ curves high or low in the event of $P(O_3)$ anomalies. Next, the MOPS 1σ uncertainty shown in Fig. 2 was relatively independent of time of day. That is, this uncertainty acts as an offset, shifting the entire median diurnal $P(O_3)$ curve either up or down, but measured $P(O_3)$ consistently exhibits the same diurnal behavior relative to the models. This result was observed for a range of atmospheric conditions: for both hot, dry and cool, high humidity days as well as for higher and lower NO days. For low NO days (NO $\leq$ 1 ppbv), median $P(O_3)$ between the MOPS and models were in closer agreement, but MOPS $P(O_3)$ still exhibited maxima before that modeled in the early morning. Finally, the observed $P(O_3)$ peak values were often much greater than the MOPS 1σ absolute uncertainty on individual days as seen in Fig.1, where differences between the MOPS and modeled $P(O_3)$ were typically between 10-20 ppbv h^{-1}. Thus, all of these results provide confidence in the robustness of the MOPS behavior relative to the models in Figs. 1 and 2.

3.3 Model-measurement $P(O_3)$ discrepancies

3.3.1 MOPS chamber artifacts

We explore several reasons for model-measurement disagreement during the morning hours. One hypothesis is that the MOPS $P(O_3)$ is positively biased due to environmental chamber chemistry artifacts: that is, offgassing of NO_2 or other chemical species from the chamber walls. At higher relative humidity, species adsorption onto these environmental chamber walls can be higher (Wainman et al., 2001) and it is possible that subsequent desorption of NO_2 or chemical species from the walls can induce artificial chemistry in the MOPS chambers.

Wall effects in the MOPS chambers can create both positive and negative fluctuations in observed $P(O_3)$. However, as described earlier, the MOPS chamber airflow is significantly higher along the walls of the MOPS chambers where surface reactions are most likely to occur. All chamber air closest to the walls is exhausted, leaving mostly center flow to be sampled by the MOPS O_3 analyzer. This airflow design, along with laboratory and atmospheric observations of chamber O_x losses less than or equal to 5%, suggests that off-gassing of O_x or other species from the MOPS chamber walls likely plays a negligible role in larger measured-than-modeled $P(O_3)$ (Cazorla and Brune, 2010; Baier et al., 2015). From the laboratory and chamber

Atmos. Chem. Phys. Discuss., doi:10.5194/acp-2016-1089, 2017
Manuscript under review for journal Atmos. Chem. Phys.
Published: 4 January 2017

Atmospheric Chemistry and Physics Discussions

testing to date, a significant loss of NO in the MOPS chambers has not been identified. Additionally, while adsorbed NO_2 can result in heterogeneous formation of nitrous acid (HONO), and a photolytic HONO source within the chambers can also result in excess $P(O_3)$ from artificial OH production (Baier et al., 2015), we calculate that this artifact during the 2014 DISCOVER-AQ campaign yields a maximum bias (3.5-7 ppbv h^{-1}) that is substantially lower than most daily MOPS $P(O_3)$ deviations from modeled $P(O_3)$ observed in Fig. 1. Therefore, in order to explain observed and modeled $P(O_3)$ differences, excess $P(O_3)$ from HONO production would need to be approximately three to five times larger than has been observed within the MOPS chambers. As mentioned earlier, higher morning $P(O_3)$ calculated from measured HO_2 has been observed at high NO with a variety of measurement methods. The MOPS observations are independent of these previous studies, but yield similar results for the dependence of $P(O_3)$ on NO, providing confidence that higher observed $P(O_3)$ is not due to significant chamber artifacts, but instead to possible differences in the chemistry between models and the MOPS measurements.

3.3.2 Influential model parameters

Model $P(O_3)$ uncertainty has been found to be slightly larger during the morning hours when differences between measured and modeled $P(O_3)$ were observed. Furthermore, model $P(O_3)$ uncertainty can possibly shift the designation of O_3 NO_x-VOC sensitivity (Chen and Brune (2012) and references therein). In order to explain calculated $P(O_3)$ behavior relative to the MOPS during hours of the day when there is typically a shift from VOC- to NO_x-sensitive $P(O_3)$ regimes, we explore model sensitivity to various inorganic and organic chemical species, reaction rates, product yields, and other model parameters outlined in supplementary material.

As described earlier, the RACM2 inputs and parameters affecting model $P(O_3)$ uncertainty are determined based on a RS-HDMR sensitivity analysis. Model uncertainty between 0600 and 1800 LT is similar between both chemical mechanisms (Table S4); the average modeled $P(O_3)$ uncertainty from RACM2 and MCMv331 is highest between 0600-1200 LT with a 1σ value of 31%, and decreases slightly to 29% between 1200 and 1800 LT. Thus, due to similar model behavior and diurnal uncertainty estimates between the RACM2 and the MCMv331, we expect that the influential inputs between the two mechanisms – model constraints and parameters contributing largely to calculated $P(O_3)$ uncertainty – will also be similar.

Model influential inputs are specific to both location and available measurements. However, many constraints that contributed to $P(O_3)$ uncertainty in Golden, CO were found to be similar to prior sensitivity analyses of chemical mechanisms conducted in much different environments (Chen and Brune (2012) and references therein). For example, two parameters consistently identified as having high importance for daytime $P(O_3)$ uncertainty involve the reaction rates, k_{OH+NO_2} and k_{HO_2+NO}, which dictate HO_x-NO_x cycling and the production and loss of HO_x. Thus, even though the uncertainty factors for these parameters are relatively low at 1.3 and 1.15 respectively (Sander et al., 2011), this important result suggests that greater emphasis should be placed on quantifying the uncertainty in HO_x-NO_x cycling reaction rates to reduce model $P(O_3)$ uncertainty.

Other model constraints influential in dictating model $P(O_3)$ uncertainty such as reaction rates, product yields and mixing ratios of species were more specific to time of day. Similar to overall results in Chen and Brune (2012), and in addition to HO_x-NO_x reaction rates, early morning $P(O_3)$ uncertainty was attributed to reaction rates involving the oxidation of reactive

Atmos. Chem. Phys. Discuss., doi:10.5194/acp-2016-1089, 2017
Manuscript under review for journal Atmos. Chem. Phys.
Published: 4 January 2017

Atmospheric Chemistry and Physics Discussions

VOCs such as aldehydes and xylenes that initiate O_3 formation propagation and produce HO_x. Additional Golden influential reaction rates involved the decomposition and formation rates of peroxyacyl nitrates (PAN), a NO_x reservoir. As O_3 increases in the afternoon, additional rates and product yields of reactions involving O_3 loss also become important, along with those between NO and other organic peroxyl species (RO_2) that continue O_3 formation. As expected, model inputs and parameters involving the formation of RO_2 or new NO_2 outside of the NO_x PSS that further propagate the O_3 formation cycle, along with inputs and parameters involving production of HO_x species, are all factors influencing model $P(O_3)$ uncertainty. Therefore, although model uncertainty is not large enough to explain model $P(O_3)$ behavior relative to the MOPS, decreasing uncertainty in model inputs, especially HO_x-NO_x reaction rates, may help to decrease total model $P(O_3)$ uncertainty and improve morning agreement between observed and modeled $P(O_3)$ in Figs. 1 and 2.

3.3.3 HO_2 versus NO

Model chemistry plays a large role in calculated $P(O_3)$ uncertainty. Therefore, we examine the chemical features driving early morning modeled-to-measured $P(O_3)$ discrepancies at high NO. Campaign median NO mixing ratios typically peaked between 0900-1100 LT at about 2 ppbv with maxima as high as 7 ppbv. As the largest differences in measured and modeled $P(O_3)$ occur during this time period when NO is greater than 1 ppbv, and HO_x-NO_x cycling reactions are significant in dictating model $P(O_3)$ uncertainty, we first examine cycling of HO_x as a function of NO.

Measurements of HO_2 and OH were made on board the NSF/NCAR C-130 using chemical ionization mass spectrometry (CIMS) with 35% and 45% accuracy (2σ), respectively (Mauldin et al., 2003; Hornbrook et al., 2011). One hypothesis for lower modeled $P(O_3)$ in the early morning is that modeled HO_2 is underestimated at high NO. Similar to prior studies (Faloona et al., 2000; Martinez et al., 2003; Ren et al., 2003; Shirley et al., 2006; Emmerson et al., 2007; Kanaya et al., 2007; Dusanter et al., 2009; Sheehy et al., 2010; Chen et al., 2010; Ren et al., 2013; Brune et al., 2015), Fig. 3 indicates that the CIMS HO_2/OH ratio is approximately equal to the modeled HO_2/OH ratio for NO less than 1 ppbv, but surpasses modeled HO_2/OH for NO greater than 1 ppbv, declining less rapidly than models for increasing NO mixing ratios. As the C-130 aircraft and continuous ground-based inorganic and organic species mixing ratios in Golden are similar, this result indicates a disagreement between measured and modeled HO_x at high NO. While previous studies have shown that measured and modeled OH at high NO are in rough agreement, differences in HO_2 were more severe (Shirley et al., 2006; Kanaya et al., 2007; Dusanter et al., 2009; Sheehy et al., 2010; Ren et al., 2013; Czader et al., 2013; Brune et al., 2015)

Figure 4 indicates $P(O_3)$ as a function of NO levels and time of day. Similar to Cazorla et al. (2012), both measured and modeled diel $P(O_3)$ increased between 0600-0800 LT during morning rush hour, peaked before 1200 LT, and then decreased later in the day with decreasing NO and VOC radical abundances. Occasional, secondary $P(O_3)$ peaks were exhibited between 1400-1600 LT in both measured and modeled $P(O_3)$, likely due to advection of O_3 precursors from the Denver region or increased local traffic emissions. Measured and modeled $P(O_3)$ dependency on NO will typically follow $P(HO_x)$ curves. Since the models were constrained by observed VOCs and NO_x, higher measured than modeled HO_2 at high NO was evident as MOPS $P(O_3)$ peaked for NO between 3-6 ppbv and modeled $P(O_3)$ peaked for NO close to 1 ppbv. This result is presumably for the same atmospheric $P(HO_x)$ regimes. If the MOPS accurately portrays net $P(O_3)$ behavior, these observations suggest

Atmos. Chem. Phys. Discuss., doi:10.5194/acp-2016-1089, 2017
Manuscript under review for journal Atmos. Chem. Phys.
Published: 4 January 2017

Atmospheric Chemistry and Physics Discussions

that chemical mechanisms may not be simulating modeled HO_x-NO_x cycling correctly. Thus, models may require further re-examination of the HO_x-NO_x rate coefficients mentioned above, or identification of possible missing reactions involving these two species groups.

3.3.4 Mechanism HO_x-NO_x chemistry

The missing modeled $P(O_3)$ between 0900-1200 LT appears to be approximately linear with NO. A missing HO_x source linearly scalable to NO that was not included in the models is plausible. However, 42 total C_2-C_{10} VOCs were measured by whole-air canister samples, representing a large suite of organic chemical species within the models, including ones with high OH reactivities that are particularly important for O_3 formation. Therefore, both of the model chemical mechanisms incorporate the dependence of VOC reactivity on NO.

Measurements of VOC reactivity were not available during the field campaign time period and thus are unavailable for comparison to modeled VOC reactivity. However, if a VOC HO_x source co-emitted with NO is missing in the models, it would have to provide an additional HO_2 source of approximately 3x10^7 radicals cm^{-3}, derived from the average difference between median diel modeled and measured $P(O_3)$. Such a missing VOC source was not identified in this study, nor has one been identified in other environments where missing HO_2 was of similar magnitude, even when proposed missing VOCs were added to model base scenarios (Martinez et al., 2003; Kanaya et al., 2007; Dusanter et al., 2009). Further, Brune et al. (2015) discuss that, if this missing HO_x source is also a missing OH loss, then this loss would be evidenced in measurements of OH reactivity at high NO, yet no such OH loss was observed.

Peroxynitric acid (HO_2NO_2), which is tied to HO_x and NO_x, is also elevated compared to models at high NO or NO_x (Spencer et al., 2009). Peroxynitric acid thermally decomposes to form HO_2 and NO_2, and can also be weakly photolyzed to form HO_2. Kanaya et al. (2007) propose that increasing the thermal decomposition rate of HO_2NO_2 could resolve model underestimation of HO_2 at high NO, but even when this decomposition rate was increased by a factor of five, it did not correct for higher measured than modeled $P(O_3)$ at high NO. Model sensitivity runs for Golden, CO using this increased decomposition rate for HO_2NO_2 in MCMv331 corroborate this same result (Fig. S2).

One reaction proposed in Brune et al. (2015) that may be able to explain observed-to-modeled $P(O_3)$ disagreement at high NO_x involves the following:

$$OH + NO + O_2 \longrightarrow HO_2 + NO_2 \cdot \quad \{1\}$$

Many studies have determined that the reaction between OH and NO to form HONO proceeds at a rate of about 4x10^{-11} cm^3 molec^{-1} s^{-1} (Sander et al. (2011) and references therein). Staikova et al. (2002) have shown that it is possible for molecular oxygen (O_2) to react with vibrationally-excited HONO to form HO_2 and NO_2. However, this reaction would have to proceed with a much slower rate than 4x10^{-11} cm^3 molec^{-1} s^{-1} and is only a minor pathway to formation of HO_2 and NO_2. Glowacki et al. (2012) have found that O_2 can react with 25% of excited-state adducts in the OH+acetylene reaction before vibrational

Atmos. Chem. Phys. Discuss., doi:10.5194/acp-2016-1089, 2017
Manuscript under review for journal Atmos. Chem. Phys.
Published: 4 January 2017

Atmospheric Chemistry and Physics Discussions

quantum state relaxation. In other studies, the formation of the hydrotrioxyl radical (HO_3) was also found to react with O_2, but due to the low-calculated HO_3 abundance in the troposphere, this radical may also be a minor pathway to HO_2. Although the reaction HO_3+NO to form HO_2+NO_2 is exothermic, it, to our knowledge, has not been tested (Murray et al., 2008; Le Picard et al., 2010; Burgess Jr, 2016). Therefore, the role of O_2 reactions with excited-state intermediates to form HO_2 in the presence of NO remains an open question. We explore the possibility of such a reaction between OH, NO, and O_2.

The OH + NO (+ O_2) reaction above has been added to the MCMv331 assuming constant atmospheric O_2 levels and varying an effective bimolecular reaction rate between (3-15)x10^{-11} cm^3 $molecule^{-1}$ s^{-1}. The modeled HO_2/OH dependence on NO closely matches those observed in Fig. 3 when a rate between (9-15)x10^{-11} cm^3 $molecule^{-1}$ s^{-1} is used. Further, with this modified chemical mechanism, modeled P(O_3) approaches median observed P(O_3) with a maximum rate between 1000-1200 LT reaching 10 ppbv h^{-1} (Fig. S2). The modeled diurnal curve then decreases later in the day similar to the median P(O_3) diel curve presented in Fig. 2. The improved agreement between measured and modeled HO_2/OH and P(O_3) behavior suggests that this reaction scheme is worth examining in more detail.

3.3.5 Reactive chlorine chemistry

Other hypotheses for model underestimation of P(O_3) relative to observations at high NO were explored, including the impacts of the under-representation of nitryl chloride ($ClNO_2$) production in current chemical mechanisms. Nitryl chloride serves as a nocturnal NO_x reservoir and, when photolyzed, can produce additional reactive chlorine (Cl) and nitrogen dioxide (NO_2). Reactive chlorine, even at low mixing ratios, has been found to serve as a major oxidant for VOCs, possibly increasing HO_2 and O_3 production in the early morning hours by as much as 30% (Finlayson-Pitts et al., 1989; Atkinson et al., 1999; Chang et al., 2002; Osthoff et al., 2008). The effects of $ClNO_2$ production on chlorine chemistry and VOC oxidation have been provided in the literature as one possible explanation for measured versus modeled HO_2 differences at higher NO levels (Thornton et al., 2010; Riedel et al., 2014; Xue et al., 2015).

Heterogeneous uptake of dinitrogen pentoxide (N_2O_5) on chloride-containing aerosol particles can produce nitric acid (HNO_3) and $ClNO_2$ in both marine and continental environments through the following reaction:

$$N_2O_5 \xrightarrow{k_{het}} \phi ClNO_2 + (2 - \phi)HNO_3, \quad \{2\}$$

where k_{het} is the heterogeneous reaction rate coefficient dependent upon the aerosol surface area density and the N_2O_5 uptake coefficient on chloride-containing aerosols, and ϕ is the $ClNO_2$ product yield.

To test this hypothesis, we constrained the MCMv331 with continuous, cavity ring-down spectroscopy measurements of N_2O_5 (Brown et al., 2002) from a nearby measurement site (Boulder Atmospheric Observatory; 40.050^{o}N, 105.010^{o}W), and implemented a reduced chlorine chemical mechanism in the MCMv331 provided by Riedel et al. (2014). We assumed an N_2O_5 uptake coefficient of 0.02, which is within the range of coefficients calculated in prior field studies (Wagner et al., 2013; Riedel et al., 2013) and laboratory experiments (Zetzsch and Behnke, 1992; Behnke et al., 1997). To be consistent with

Atmos. Chem. Phys. Discuss., doi:10.5194/acp-2016-1089, 2017
Manuscript under review for journal Atmos. Chem. Phys.
Published: 4 January 2017

Atmospheric Chemistry and Physics Discussions

previous studies near Golden, the aerosol surface area density was varied between 150 and 250 μm^2 cm^{-3}, and ϕ is varied between 0.05 and 0.1 (Thornton et al., 2010; Riedel et al., 2013). It is important to note that these assumptions vary largely with relative humidity and aerosol surface area and composition (Thornton and Abbatt, 2005; Bertram and Thornton, 2009; Roberts et al., 2009; Thornton et al., 2010; Wagner et al., 2013; Riedel et al., 2013), but modeling over a range of values can provide a qualitative prediction of $ClNO_2$ production effects on model $P(O_3)$ in this region. In each model case, the MCMc331 runs including $ClNO_2$ production and Cl-VOC chemistry resulted in average $ClNO_2$ mixing ratios between 0.04 and 0.13 ppbv during the early morning hours (0300-0600 LT) and a slight increase in diurnal $P(O_3)$ values of less than 5%. Thus, although chlorine chemistry can have a large effect on $P(O_3)$ during the winter and for marine environments, these model runs indicate that Cl chemistry does not play a large enough role in O_3 photochemistry during this summer campaign to explain the morning observed discrepancy between measured and modeled O_3 formation rates in Golden, CO.

3.3.6 Nitrous acid photolysis

Perhaps more of an important HO_x source in the morning hours at high NO or NO_x than $ClNO_2$ is the production and photolysis of HONO. Other important HO_x sources include hydrogen peroxide and organic VOC photolysis, and O_3 photolysis followed by the subsequent reaction between $O(^1D)$ and water vapor to produce OH. In previous field studies, HONO photolysis contributed largely to the daytime HO_x production (Alicke et al., 2003; Ren et al., 2003; Kanaya et al., 2007; Dusanter et al., 2009; Volkamer et al., 2010; Ren et al., 2013).

Nitrous acid was not measured during DISCOVER-AQ or FRAPPÉ, and was thus predicted by the RACM2 and MCMv331 based on continuous, ground-based NO_x observations. Therefore, model under-prediction of HONO mixing ratios in the morning can be one cause for modeled versus measured HO_2/OH disagreement. However, studies in which HONO was continuously measured and used to constrain both zero-dimensional and three-dimensional chemical models still exhibited the same behavior of higher measured than modeled HO_2 to OH ratios at high NO (Ren et al., 2003; Martinez et al., 2003; Dusanter et al., 2009; Chen et al., 2010; Czader et al., 2013; Ren et al., 2013; Brune et al., 2015). Thus, this morning HO_x source is likely not the sole cause for model under-prediction of model HO_2 – and thus, $P(O_3)$ – at high NO_x found here and in previous studies.

3.4 Implications for O_3 mitigation strategies

3.4.1 NO_x-VOC sensitivity

The underestimation of model $P(O_3)$ relative to the MOPS at high NO or NO_x can have far-reaching implications for model assessment of the dependency of $P(O_3)$ on NO_x and VOCs. The fraction of free radicals removed by NO_x, L_N/Q, has been used in the literature to assess NO_x-VOC sensitivity in regions experiencing high O_3 (Daum et al., 2004; Kleinman, 2005; Ren et al., 2013). Here, L_N is the rate of total free radical removal by NO_x, and Q is the total radical production rate. When significantly above 0.5, the atmosphere is within a VOC-sensitive regime, while when significantly below 0.5, the atmosphere is within a NO_x-sensitive regime (Kleinman, 2005). The median L_N/Q was calculated with the RACM2 using full-campaign observations, indicating that Golden $P(O_3)$ is VOC-sensitive before 1200 LT, and NO_x-sensitive thereafter according to models

Atmos. Chem. Phys. Discuss., doi:10.5194/acp-2016-1089, 2017
Manuscript under review for journal Atmos. Chem. Phys.
Published: 4 January 2017

Atmospheric Chemistry and Physics Discussions

(Fig. S3). During DISCOVER-AQ and FRAPPÉ, model sensitivity studies conducted for the Boulder Atmospheric Observatory site just northeast of Golden also found maximum photochemical O_3 to be largely NO_x-sensitive in the afternoon (McDuffie et al., 2016). However, if HO_2 is underestimated by chemical mechanisms such as the RACM2 and the MCMv331, the total radical production rate, Q, may also be underestimated, thereby shifting the NO_x-VOC sensitivity more towards a NO_x-sensitive regime. Model runs including the proposed OH + NO reaction indicate a shift from VOC- to NO_x-sensitive conditions approximately one to two hours earlier in the morning than base-case model chemistry (Fig. S3).

The largest O_3 formation rates are measured before 1200 LT when NO_x and VOC emissions are high and the mixing layer is relatively shallow. Although a shallow mixing layer is one reason for high MOPS $P(O_3)$ during the morning hours, we note that secondary diurnal MOPS $P(O_3)$ peaks are also evidenced on individual days alongside increased NO_x and VOCs during afternoon rush hour in a deeper mixing layer. Further, high $P(O_3)$ and the shift from VOC- to NO_x-sensitive O_3 formation in the late morning could be attributed to early-morning entrainment of VOCs from the free troposphere in the absence of NO_x entrainment. However, these VOCs in the upper troposphere are longer-lived and are less important in propagating O_3 formation than other, higher reactivity VOCs. Therefore, although entrainment of species during the morning hours and the depth of the mixing layer influence NO_x-VOC sensitivity and these high morning $P(O_3)$ rates, it is more likely that O_3 precursor species at the surface level predominantly influence observed $P(O_3)$ for this study.

Generally speaking, while longer-term analyses are required to suggest effective O_3 reduction strategies for Golden and surrounding regions, if the $P(O_3)$ NO_x-VOC sensitivity is shifted more towards a NO_x-sensitive regime in the morning as the MOPS observations suggest, reducing NO_x may be an effective strategy for O_3 mitigation in the Colorado Front Range.

3.4.2 O_x advection

Ozone formation precursors can be transported westward to Golden because of the Colorado Front Range terrain and its induced wind patterns. When air in Golden is influenced by O_3 precursor emissions from the east (e.g. the Denver metropolitan and Commerce City regions), greater anthropogenic VOC and NO mixing ratios are measured on average. Thus, we evaluate calculated O_3 advection using Eq. (1) in an attempt to evaluate the impact of O_3 advection derived from the MOPS and the models on observed O_3 patterns in Golden.

Measured O_x maxima are 2-7 ppbv greater on these “plume" days than when air is advected from elsewhere, and higher $P(O_3)$ is measured by the MOPS than is modeled by the RACM2 and MCMv331 (Fig. 5). When winds are not easterly (“non-plume" days), lower levels of anthropogenic VOCs, NO, and O_x maxima are observed, and average measured diel $P(O_3)$ is 45% lower than on plume days. This MOPS behavior stands in contrast to the models, where average diel RACM2 and MCMv331 $P(O_3)$ is approximately 30% lower on plume days than all other days. A simple advection analysis was performed to determine the factors in Eq. (1) that most likely contribute to observed O_x levels in Fig. 5 for plume and non-plume days. The transport rate of O_x out of the mixing layer through deposition is calculated to be at most 1 ppbv h^{-1} and is neglected here. The morning O_3 entrainment rate during DISCOVER-AQ and FRAPPE has been calculated for the Colorado Front Range region to be 5 ppbv h^{-1} on average, with afternoon average entrainment rates of approximately -1 ppbv h^{-1} (Kaser et al. (2016), *in prep*). Assuming an average entrainment rate of 5 ppbv h^{-1} for morning hours between 0600-1200 LT and an O_x entrainment rate

Atmos. Chem. Phys. Discuss., doi:10.5194/acp-2016-1089, 2017
Manuscript under review for journal Atmos. Chem. Phys.
Published: 4 January 2017

Atmospheric Chemistry and Physics Discussions

of -1 ppbv h^{-1} for times between 1200-1800 LT and subtracting diel entrainment and observed P(O_x) from the local diel O_x rate of change, the average O_x advection rate derived from MOPS and models between 0600-1800 LT is -5.1 and -2.4 ppbv h^{-1} on plume days, and -1.7 and -3.5 ppbv h^{-1} for all other days, respectively. This quick calculation suggests that advection contributes weakly to observed O_x, while either entrainment or P(O_x) dominate the O_x patterns observed in Golden and likely its surrounding areas. Because these advection rates are derived quantities from the MOPS and the models, and both methods for determining P(O_x) contain relatively high uncertainty, it is difficult to quantitatively assess O_x advection rates in Golden, CO as these errors propagate to advection rate uncertainties of up to a factor of two. Decreasing the uncertainty in P(O_x) is thus salient for accurately calculating the terms in Eq. (1) contributing to observed O_x levels in the Colorado Front Range.

4 Conclusions

Comparisons were made between P(O_3) measured *in situ* by a second-generation Penn State MOPS, and photochemical box modeled P(O_3) using both lumped and near-explicit chemical mechanisms. These 2014 comparisons during DISCOVER-AQ and FRAPPÈ in the Colorado Front Range show that model P(O_3) is underestimated relative to the MOPS by a factor of two. This underestimation is most pronounced between 0900 and 1200 LT during peak O_3 production hours when high levels of NO_x and VOCs are present due to rush hour emissions.

This result is not completely explained by several different possibilities. Model P(O_3) uncertainty is large during peak P(O_3) hours; factors influencing this uncertainty during the day include uncertainty in the kinetic rate coefficients of HO_x-NO_x cycling reactions. Upon further analysis of the discrepancy between measured and modeled P(O_3) at high NO_x, it was found that the measured HO_2 behavior as a function of NO was similar to studies previously reported in the literature in which the measured HO_2 to OH ratio decreases less rapidly than modeled ratios for higher NO levels, most likely causing P(O_3) measured by the MOPS to be up to 2-3 times larger than modeled P(O_3) between 0900 and 1200 LT. As such, neither MOPS chamber chemistry, reactive chlorine chemistry, nor model sensitivity studies can fully explain this disagreement between modeled and measured P(O_3). If we include a reaction of OH + NO to form HO_2 and NO_2 with a bimolecular reaction rate coefficient of (9-15)x10^{-11} cm^3 $molec^{-1}$ s^{-1}, the model can replicate the MOPS observed P(O_3) behavior in this Golden, CO study.

More research must be conducted on both fronts to understand the differences between modeled and measured P(O_3). The second-generation MOPS is still in early stages of development and much more time and rigorous testing is needed to decrease the MOPS absolute measurement offset uncertainty through the reduction of O_3 analyzer drifting. On the other hand, model comparisons highlight the need to revisit current mechanism reaction rate coefficients and product yields involving HO_x-NO_x cycling, and to investigate possible missing HO_x sources at high NO_x levels.

If models are truly under-predicting HO_2 in the early morning, L_N/Q metrics from observation-constrained models that calculate radical mixing ratios may be incorrectly assessing NO_x or VOC O_3 production sensitivity and the efficacy of O_3 reduction strategies. Further, the use of these mechanisms in CTMs can create significant differences between modeled and observed P(O_3) during peak O_3 production hours and can translate to large discrepancies in model O_3 predictions. Thus, differences between measured and modeled P(O_3) can have substantial and potentially costly implications for O_3 mitigation

Atmos. Chem. Phys. Discuss., doi:10.5194/acp-2016-1089, 2017
Manuscript under review for journal Atmos. Chem. Phys.
Published: 4 January 2017

Atmospheric Chemistry and Physics Discussions

strategies that are put in place in O_3 NAAQS non-attainment areas. The MOPS measurements indicate $P(O_3)$ in Golden, CO and its surrounding areas are more NO_x-sensitive in the early morning, suggesting that NO_x emission reductions in this region are a viable solution for O_3 mitigation in the Colorado Front Range.

5 Data availability

The MCM version 3.3.1 is freely available at http://mcm.leeds.ac.uk/MCM/ and the University of Washington Chemical Model (UWCM) framework used to run MCMv331 is available to the public from G. Wolfe. Meteorological and chemical data collected during the DISCOVER-AQ and FRAPPÈ studies are available at http://www-air.larc.nasa.gov/missions/discover-aq/discover-aq.html and https://www2.acom.ucar.edu/frappe.

Author S. Brown serves on the editorial board of this journal. No other authors declare any conflicts of interest.

Acknowledgements. We gratefully acknowledge the entire DISCOVER-AQ and FRAPPÈ teams for the collection of ground and airborne measurement data in this work. PTR-ToF-MS measurements during DISCOVER-AQ were carried out by P. Eichler, T. Mikoviny, and M. Müller, and were supported by the Austrian Federal Ministry for Transport, Innovation and Technology (bmvit) through the Austrian Space Applications Programme (ASAP) of the Austrian Research Promotion Agency (FFG). We thank G. Wolfe for provision of and help with the MCM model framework, W. Goliff for the provision of the RACM2, and J. Thornton for thoughtful discussions. For the use of the web version of the HYSPLIT model (http://www.ready.noaa.gov), we acknowledge the NOAA Air Resources Laboratory. This work was funded by NASA grants NNX14AR83G and NNX12AB84G.

Atmos. Chem. Phys. Discuss., doi:10.5194/acp-2016-1089, 2017
Manuscript under review for journal Atmos. Chem. Phys.
Published: 4 January 2017

Atmospheric Chemistry and Physics Discussions

References

Alicke, B., Geyer, A., Hofzumahaus, A., Holland, F., Konrad, S., Pätz, H., Schäfer, J., Stutz, J., Volz-Thomas, A., and Platt, U.: OH formation by HONO photolysis during the BERLIOZ experiment, Journal of Geophysical Research: Atmospheres, 108, 2003.

Apel, E., Hills, A., Lueb, R., Zindel, S., Eisele, S., and Riemer, D.: A fast-GC/MS system to measure C2 to C4 carbonyls and methanol aboard aircraft, Journal of Geophysical Research: Atmospheres, 108, 2003.

Appel, K. W., Gilliland, A. B., Sarwar, G., and Gilliam, R. C.: Evaluation of the Community Multiscale Air Quality (CMAQ) model version 4.5: Sensitivities impacting model performance: Part I: Ozone, Atmospheric Environment, 41, 9603–9615, doi:10.1016/j.atmosenv.2007.08.044, http://www.sciencedirect.com/science/article/pii/S1352231007007534, 2007.

Atkinson, R., Baulch, D., Cox, R., Hampson Jr, R., Kerr, J., Rossi, M., and Troe, J.: Evaluated kinetic and photochemical data for atmospheric chemistry, organic species: Supplement VII, Journal of Physical and chemical reference Data, 28, 191–393, 1999.

Baier, B. C., Brune, W. H., Lefer, B. L., Miller, D. O., and Martins, D. K.: Direct ozone production rate measurements and their use in assessing ozone source and receptor regions for Houston in 2013, Atmospheric Environment, 114, 83–91, doi:10.1016/j.atmosenv.2015.05.033, http://www.sciencedirect.com/science/article/pii/S1352231015301060, 2015.

Banta, R. M.: Daytime Boundary-Layer Evolution over Mountainous Terrain. Part 1: Observations of the Dry Circulations, Mon. Wea. Rev., 112, 340–356, doi:10.1175/1520-0493(1984)112<0340:DBLEOM>2.0.CO;2, http://journals.ametsoc.org/doi/abs/10.1175/1520-0493(1984)112%3C0340%3ADBLEOM%3E2.0.CO%3B2, 1984.

Behnke, W., George, C., Scheer, V., and Zetzsch, C.: Production and decay of ClNO2 from the reaction of gaseous N2O5 with NaCl solution: Bulk and aerosol experiments, J. Geophys. Res., 102, 3795–3804, doi:10.1029/96JD03057, http://onlinelibrary.wiley.com/doi/10.1029/96JD03057/abstract, 1997.

Bell, M. L., McDermott, A., Zeger, S., Samet, J., and Dominici, F.: Ozone and Short-term Mortality in 95 US Urban Communities 1987-2000, Journal of the American Medical Association, 292, doi:10.1001/jama.292.19.2372, 2004.

Bertram, T. H. and Thornton, J. A.: Toward a general parameterization of N2O5 reactivity on aqueous particles: the competing effects of particle liquid water, nitrate and chloride, Atmos. Chem. Phys., 9, 8351–8363, doi:10.5194/acp-9-8351-2009, http://www.atmos-chem-phys.net/9/8351/2009/, 2009.

Bloss, C., Wagner, V., Jenkin, M. E., Volkamer, R., Bloss, W. J., Lee, J. D., Heard, D. E., Wirtz, K., Martin-Reviejo, M., Rea, G., Wenger, J. C., and Pilling, M. J.: Development of a detailed chemical mechanism (MCMv3.1) for the atmospheric oxidation of aromatic hydrocarbons, Atmospheric Chemistry and Physics, 5, 641–664, doi:10.5194/acp-5-641-2005, http://www.atmos-chem-phys.net/5/641/2005/, 2005.

Brown, S. S., Stark, H., Ciciora, S. J., McLaughlin, R. J., and Ravishankara, A.: Simultaneous in situ detection of atmospheric NO3 and N2O5 via cavity ring-down spectroscopy, Review of scientific instruments, 73, 3291–3301, 2002.

Brune, W. H., Baier, B. C., Thomas, J., Ren, X., Cohen, R., Pusede, S. E., Browne, E., Goldstein, A., Gentner, D. R., Keutsch, F. N., Thornton, J. A., Harrold, S., Lopez-Hilfiker, F., and Wennberg, P. O.: Ozone Production Chemistry in the Presence of Urban Plumes, Faraday Discuss., doi:10.1039/C5FD00204D, http://pubs.rsc.org/en/content/articlelanding/2015/fd/c5fd00204d, 2015.

Burgess Jr, D. R.: An Evaluation of Gas Phase Enthalpies of Formation for Hydrogen-Oxygen (Hˆ sub xˆ Oˆ sub yˆ) Species, Journal of Research of the National Institute of Standards and Technology, 121, 108, 2016.

Calvert, J. G., Orlando, J. J., Stockwell, W. R., and Wallington, T. J.: The Mechanisms of Reactions Influencing Atmospheric Ozone, Oxford University Press, 2015.

Cazorla, M. and Brune, W. H.: Measurement of Ozone Production Sensor, Atmospheric Measurement Techniques, 3, 545–555, doi:10.5194/amt-3-545-2010, 2010.

Cazorla, M., Brune, W. H., Ren, X., and Lefer, B.: Direct measurement of ozone production rates in Houston in 2009 and comparison with two estimation methods, Atmos. Chem. Phys., 12, 1203–1212, doi:10.5194/acp-12-1203-2012, 2012.

Chang, S., McDonald-Buller, E., Kimura, Y., Yarwood, G., Neece, J., Russell, M., Tanaka, P., and Allen, D.: Sensitivity of urban ozone formation to chlorine emission estimates, Atmospheric Environment, 36, 4991–5003, 2002.

Chen, S. and Brune, W. H.: Global sensitivity analysis of ozone production and O3-NOx-VOC limitation based on field data, Atmospheric Environment, 55, 288–296, doi:10.1016/j.atmosenv.2012.03.061, 2012.

Chen, S., Ren, X., Mao, J., Chen, Z., Brune, W. H., Lefer, B., Rappenglück, B., Flynn, J., Olson, J., and Crawford, J. H.: A comparison of chemical mechanisms based on TRAMP-2006 field data, Atmospheric Environment, 44, 4116–4125, doi:10.1016/j.atmosenv.2009.05.027, 2010.

Chen, S., Brune, W. H., Oluwole, O. O., Kolb, C. E., Bacon, F., Li, G., and Rabitz, H.: Global sensitivity analysis of the regional atmospheric chemical mechanism: an application of random sampling-high dimensional model representation to urban oxidation chemistry, Environmental science & technology, 46, 11 162–11 170, doi:10.1021/es301565w, PMID: 22963531, 2012.

Colman, J. J., Swanson, A. L., Meinardi, S., Sive, B. C., Blake, D. R., and Rowland, F. S.: Description of the analysis of a wide range of volatile organic compounds in whole air samples collected during PEM-Tropics A and B, Analytical Chemistry, 73, 3723–3731, 2001.

Crilley, L., Kramer, L., Pope, F. D., Whalley, L. K., Cryer, D. R., Heard, D. E., Lee, J., Reed, C., and Bloss, W.: On the interpretation of in situ HONO observations via photochemical steady state, Faraday Discussions, 2016.

Czader, B. H., Li, X., and Rappenglueck, B.: CMAQ modeling and analysis of radicals, radical precursors, and chemical transformations, J. Geophys. Res. Atmos., 118, 11,376–11,387, doi:10.1002/jgrd.50807, http://onlinelibrary.wiley.com/doi/10.1002/jgrd.50807/abstract, 2013.

Daum, P. H., Kleinman, L. I., Springston, S. R., Nunnermacker, L. J., Lee, Y.-N., Weinstein-Lloyd, J., Zheng, J., and Berkowitz, C. M.: Origin and properties of plumes of high ozone observed during the Texas 2000 Air Quality Study (TexAQS 2000), J. Geophys. Res., 109, D17 306, doi:10.1029/2003JD004311, http://onlinelibrary.wiley.com/doi/10.1029/2003JD004311/abstract, 2004.

Day, D., Wooldridge, P., Dillon, M., Thornton, J., and Cohen, R.: A thermal dissociation laser-induced fluorescence instrument for in situ detection of NO2, peroxy nitrates, alkyl nitrates, and HNO3, Journal of Geophysical Research: Atmospheres, 107, 2002.

Dodge, M. C.: Chemical oxidant mechanisms for air quality modeling: critical review, Atmospheric Environment, 34, 2103–2130, doi:10.1016/S1352-2310(99)00461-6, http://www.sciencedirect.com/science/article/pii/S1352231099004616, 2000.

Dusanter, S., Vimal, D., Stevens, P., Volkamer, R., and Molina, L.: Measurements of OH and HO 2 concentrations during the MCMA-2006 field campaign–Part 1: Deployment of the Indiana University laser-induced fluorescence instrument, Atmospheric Chemistry and Physics, 9, 1665–1685, 2009.

Emmerson, K., Carslaw, N., Carpenter, L., Heard, D., Lee, J., and Pilling, M.: Urban atmospheric chemistry during the PUMA campaign 1: Comparison of modelled OH and HO2 concentrations with measurements, Journal of Atmospheric Chemistry, 52, 143–164, 2005.

Emmerson, K., Carslaw, N., Carslaw, D., Lee, J., McFiggans, G., Bloss, W., Gravestock, T., Heard, D., Hopkins, J., Ingham, T., Pilling, M. J., Smith, S., Jacob, D. J., and Monks, P. S.: Free radical modelling studies during the UK TORCH Campaign in Summer 2003, 7, 167–181, http://www.atmos-chem-phys.org/7/167/2007/acp-7-167-2007.pdf, 2007.

Faloona, I., Tan, D., Brune, W. H., Jaeglé, L., Jacob, D. J., Kondo, Y., Koike, M., Chatfield, R., Pueschel, R., Ferry, G., Sachse, G., Vay, S., Anderson, B., Hannon, J., and Fuelberg, H.: Observations of HOx and its relationship with NO x in the upper troposphere during SONEX, J. Geophys. Res., 105, 3771–3783, doi:10.1029/1999JD900914, http://onlinelibrary.wiley.com/doi/10.1029/1999JD900914/abstract, 2000.

Finlayson-Pitts, B., Wingen, L., Sumner, A., Syomin, D., and Ramazan, K.: The heterogenous hydrolysis of NO2 in laboratory systems and in outdoor and indoor atmospheres: An integrated mechanism, Physical Chemistry Chemical Physics, 5, 223–242, doi:10.1039/B208564J, 2003.

Finlayson-Pitts, B. J. and Pitts, J. N.: The chemical basis of air quality- Kinetics and mechanisms of photochemical air pollution and application to control strategies, Advances in environmental science and technology., 7, 75–162, 1977.

Finlayson-Pitts, B. J., Ezell, M. J., and Pitts, J. N.: Formation of chemically active chlorine compounds by reactions of atmospheric NaCl particles with gaseous N2O5 and ClONO2, Nature, 337, 241–244, doi:10.1038/337241a0, http://www.nature.com/nature/journal/v337/n6204/abs/337241a0.html, 1989.

George, C., Strekowski, R., Kleffmann, J., Stemmler, K., and Ammann, M.: Photoenhanced uptake of gaseous NO2 on solid organic compounds: a photochemical source of HONO, Faraday Discussions, 130, 195–210, 2005.

Gilliland, A. B., Hogrefe, C., Pinder, R. W., Godowitch, J. M., Foley, K. L., and Rao, S. T.: Dynamic evaluation of regional air quality models: Assessing changes in O3 stemming from changes in emissions and meteorology, Atmospheric Environment, 42, 5110–5123, doi:10.1016/j.atmosenv.2008.02.018, http://www.sciencedirect.com/science/article/pii/S1352231008001374, 2008.

Glowacki, D. R., Lockhart, J., Blitz, M. A., Klippenstein, S. J., Pilling, M. J., Robertson, S. H., and Seakins, P. W.: Interception of excited vibrational quantum states by O2 in atmospheric association reactions, Science, 337, 1066–1069, 2012.

Goliff, W. S., Stockwell, W. R., and Lawson, C. V.: The regional atmospheric chemistry mechanism, version 2, Atmospheric Environment, 68, 174–185, doi:10.1016/j.atmosenv.2012.11.038, http://www.sciencedirect.com/science/article/pii/S1352231012011065, 2013.

Haagen-Smit, A. J., Bradley, C. E., and Fox, M. M.: Ozone Formation in Photochemical Oxidation of Organic Substances, Ind. Eng. Chem., 45, 2086–2089, doi:10.1021/ie50525a044, http://dx.doi.org/10.1021/ie50525a044, 1953.

Hornbrook, R. S., Crawford, J. H., Edwards, G. D., Goyea, O., Mauldin III, R. L., Olson, J. S., and Cantrell, C. A.: Measurements of tropospheric HO2 and RO2 by oxygen dilution modulation and chemical ionization mass spectrometry, Atmos. Meas. Tech., 4, 735–756, doi:10.5194/amt-4-735-2011, http://www.atmos-meas-tech.net/4/735/2011/, 2011.

Im, U., Bianconi, R., Solazzo, E., Kioutsioukis, I., Badia, A., Balzarini, A., Baró, R., Bellasio, R., Brunner, D., Chemel, C., et al.: Evaluation of operational on-line-coupled regional air quality models over Europe and North America in the context of AQMEII phase 2. Part I: Ozone, Atmospheric Environment, 115, 404–420, 2015.

Jaegle, L., Jacob, D. J., Brune, W. H., Tan, D., Faloona, I. C., Weinheimer, A. J., Ridley, B. A., Campos, T. L., and Sachse, G. W.: Sources of HOx and production of ozone in the upper troposphere over the United States, Geophysical Research Letters, 25, 1709–1712, doi:10.1029/98GL00041, http://dx.doi.org/10.1029/98GL00041, 1998.

Jeffries, H. E. and Tonnesen, S.: A comparison of two photochemical reaction mechanisms using mass balance and process analysis, Atmospheric Environment, 28, 2991–3003, 1994.

Jenkin, M. E., Saunders, S. M., and Pilling, M. J.: The tropospheric degradation of volatile organic compounds: a protocol for mechanism development, Atmospheric Environment, 31, 81–104, doi:10.1016/S1352-2310(96)00105-7, http://www.sciencedirect.com/science/article/pii/S1352231096001057, 1997.

Jenkin, M. E., Saunders, S. M., Wagner, V., and Pilling, M. J.: Protocol for the development of the Master Chemical Mechanism, MCM v3 (Part B): tropospheric degradation of aromatic volatile organic compounds, Atmos. Chem. Phys., 3, 181–193, doi:10.5194/acp-3-181-2003, http://www.atmos-chem-phys.net/3/181/2003/, 2003.

Jenkin, M. E., Young, J. C., and Rickard, A. R.: The MCM v3.3.1 degradation scheme for isoprene, Atmos. Chem. Phys., 15, 11 433–11 459, doi:10.5194/acp-15-11433-2015, http://www.atmos-chem-phys.net/15/11433/2015/, 2015.

Jimenez, P., Baldasano, J. M., and Dabdub, D.: Comparison of photochemical mechanisms for air quality modeling, Atmospheric Environment, 37, 4179–4194, doi:10.1016/S1352-2310(03)00567-3, 2003.

Kanaya, Y., Cao, R., Akimoto, H., Fukuda, M., Komazaki, Y., Yokouchi, Y., Koike, M., Tanimoto, H., Takegawa, N., and Kondo, Y.: Urban photochemistry in central Tokyo: 1. Observed and modeled OH and HO2 radical concentrations during the winter and summer of 2004, J. Geophys. Res., 112, D21 312, doi:10.1029/2007JD008670, http://onlinelibrary.wiley.com/doi/10.1029/2007JD008670/abstract, 2007.

Kanaya, Y., Fukuda, M., Akimoto, H., Takegawa, N., Komazaki, Y., Yokouchi, Y., Koike, M., and Kondo, Y.: Urban photochemistry in central Tokyo: 2. Rates and regimes of oxidant (O3+ NO2) production, Journal of Geophysical Research: Atmospheres, 113, 2008.

Kaser, L., Patton, E., Pfister, G. G., Weinheimer, A., and Coauthors: The effect of vertical mixing on observed and modeled surface ozone in the Colorado Front Range, *in prep*, 2016.

Kleinman, L. I.: The dependence of tropospheric ozone production rate on ozone precursors, Atmospheric Environment, 39, 575–586, doi:10.1016/j.atmosenv.2004.08.047, 2005.

Kleinman, L. I., Daum, P. H., Lee, J. H., Lee, Y.-N., Nunnermacker, L. J., Springston, S. R., Newman, L., Weinstein-Lloyd, J., and Sillman, S.: Dependence of ozone production on NO and hydrocarbons in the troposphere, Geophysical Research Letters, 24, 2299–2302, doi:10.1029/97GL02279, 1997.

Krupa, S. V. and Manning, W. J.: Toxic Substance in the Environment Atmospheric ozone: Formation and effects on vegetation, Environmental Pollution, 50, 101–137, doi:10.1016/0269-7491(88)90187-X, http://www.sciencedirect.com/science/article/pii/026974918890187X, 1988.

Kuhn, M., Builtjes, P. J. H., Poppe, D., Simpson, D., Stockwell, W. R., Andersson-Sköld, Y., Baart, A., Das, M., Fiedler, F., Hov, , Kirchner, F., Makar, P. A., Milford, J. B., Roemer, M. G. M., Ruhnke, R., Strand, A., Vogel, B., and Vogel, H.: Intercomparison of the gas-phase chemistry in several chemistry and transport models, Atmospheric Environment, 32, 693–709, doi:10.1016/S1352-2310(97)00329-4, http://www.sciencedirect.com/science/article/pii/S1352231097003294, 1998.

Langridge, J. M., Gustafsson, R. J., Griffiths, P. T., Cox, R. A., Lambert, R. M., and Jones, R. L.: Solar driven nitrous acid formation on building material surfaces containing titanium dioxide: A concern for air quality in urban areas?, Atmospheric Environment, 43, 5128–5131, 2009.

Le Picard, S. D., Tizniti, M., Canosa, A., Sims, I. R., and Smith, I. W.: The thermodynamics of the elusive HO3 radical, Science, 328, 1258–1262, 2010.

Lee, J., Whalley, L., Heard, D., Stone, D., Dunmore, R., Hamilton, J., Young, D., Allan, J., Laufs, S., and Kleffmann, J.: Detailed budget analysis of HONO in central London reveals a missing daytime source, Atmospheric Chemistry and Physics, 16, 2747–2764, 2016.

Li, G., Hu, J., Wang, S.-W., Georgopoulos, P. G., Schoendorf, J., and Rabitz, H.: Random Sampling-High Dimensional Model Representation (RS-HDMR) and Orthogonality of Its Different Order Component Functions, J. Phys. Chem. A, 110, 2474–2485, doi:10.1021/jp054148m, http://dx.doi.org/10.1021/jp054148m, 2006.

Li, G., Rabitz, H., Yelvington, P. E., Oluwole, O. O., Bacon, F., Kolb, C. E., and Schoendorf, J.: Global Sensitivity Analysis for Systems with Independent and/or Correlated Inputs, J. Phys. Chem. A, 114, 6022–6032, doi:10.1021/jp9096919, http://dx.doi.org/10.1021/jp9096919, 2010.

Luecken, D., Phillips, S., Sarwar, G., and Jang, C.: Effects of using the CB05 vs. SAPRC99 vs. CB4 chemical mechanism on model predictions: Ozone and gas-phase photochemical precursor concentrations, Atmospheric Environment, 42, 5805–5820, doi:10.1016/j.atmosenv.2007.08.056, http://www.sciencedirect.com/science/article/pii/S1352231007007728, 2008.

Luecken, D. J., Tonnesen, G. S., and Sickles, J. E., I.: Differences in NOy speciation predicted by three photochemical mechanisms, Atmospheric Environment, 33, 1073–1084, doi:10.1016/S1352-2310(98)00319-7, http://www.sciencedirect.com/science/article/pii/S1352231098003197, 1999.

Madronich, S. and Flocke, S.: The Role of Solar Radiation in Atmospheric Chemistry, in: Environmental Photochemistry, edited by Boule, D. P., no. 2 / 2L in The Handbook of Environmental Chemistry, pp. 1–26, Springer Berlin Heidelberg, http://link.springer.com/chapter/10.1007/978-3-540-69044-3_1, 1999.

Mao, J., Paulot, F., Jacob, D. J., Cohen, R. C., Crounse, J. D., Wennberg, P. O., Keller, C. A., Hudman, R. C., Barkley, M. P., and Horowitz, L. W.: Ozone and organic nitrates over the eastern United States: Sensitivity to isoprene chemistry, Journal of Geophysical Research: Atmospheres, 118, 2013.

Martinez, M., Harder, H., Kovacs, T. A., Simpas, J. B., Bassis, J., Lesher, R., Brune, W. H., Frost, G. J., Williams, E. J., Stroud, C. A., Jobson, B. T., Roberts, J. M., Hall, S. R., Shetter, R. E., Wert, B., Fried, A., Alicke, B., Stutz, J., Young, V. L., White, A. B., and Zamora, R. J.: OH and HO2 concentrations, sources, and loss rates during the Southern Oxidants Study in Nashville, Tennessee, summer 1999, Journal of Geophysical Research: Atmospheres, 108, 4617–4634, doi:10.1029/2003JD003551, 2003.

Mauldin, R. L., Cantrell, C. A., Zondlo, M., Kosciuch, E., Eisele, F. L., Chen, G., Davis, D., Weber, R., Crawford, J., Blake, D., Bandy, A., and Thornton, D.: Highlights of OH, H2SO4, and methane sulfonic acid measurements made aboard the NASA P-3B during Transport and Chemical Evolution over the Pacific : NASA global tropospheric experiment transport and chemical evolution over the Pacific (TRACE-P): Measurements and analysis (TRACEP1), Journal of geophysical research, 108, GTE17.1–GTE17.13, http://cat.inist.fr/?aModele=afficheN&cpsidt=15353084, 2003.

McDuffie, E. E., Edwards, P. M., Gilman, J. B., Lerner, B. M., Dubé, W. P., Trainer, M., Wolfe, D. E., Angevine, W. M., deGouw, J., Williams, E. J., et al.: Influence of oil and gas emissions on summertime ozone in the Colorado Northern Front Range, Journal of Geophysical Research: Atmospheres, 121, 8712–8729, 2016.

Müller, M., Mikoviny, T., Feil, S., Haidacher, S., Hanel, G., Hartungen, E., Jordan, A., Märk, L., Mutschlechner, P., Schottkowsky, R., Sulzer, P., Crawford, J. H., and Wisthaler, A.: A compact PTR-ToF-MS instrument for airborne measurements of volatile organic compounds at high spatiotemporal resolution, Atmospheric Measurement Techniques, 7, 3763–3772, doi:10.5194/amt-7-3763-2014, http://www.atmos-meas-tech.net/7/3763/2014/, 2014.

Murray, C., Derro, E. L., Sechler, T. D., and Lester, M. I.: Weakly bound molecules in the atmosphere: a case study of HOOO, Accounts of chemical research, 42, 419–427, 2008.

Olson, J., Prather, M., Berntsen, T., Carmichael, G., Chatfield, R., Connell, P., Derwent, R., Horowitz, L., Jin, S., Kanakidou, M., Kasibhatla, P., Kotamarthi, R., Kuhn, M., Law, K., Penner, J., Perliski, L., Sillman, S., Stordal, F., Thompson, A., and Wild, O.: Results from the Intergovernmental Panel on Climatic Change Photochemical Model Intercomparison (PhotoComp), J. Geophys. Res., 102, 5979–5991, doi:10.1029/96JD03380, http://onlinelibrary.wiley.com/doi/10.1029/96JD03380/abstract, 1997.

Osthoff, H. D., Roberts, J. M., Ravishankara, A. R., Williams, E. J., Lerner, B. M., Sommariva, R., Bates, T. S., Coffman, D., Quinn, P. K., Dibb, J. E., Stark, H., Burkholder, J. B., Talukdar, R. K., Meagher, J., Fehsenfeld, F. C., and Brown, S. S.: High levels of nitryl chloride in the polluted subtropical marine boundary layer, Nature Geosci, 1, 324–328, doi:10.1038/ngeo177, http://www.nature.com/ngeo/journal/v1/n5/full/ngeo177.html, 2008.

Paulot, F., Crounse, J., Kjaergaard, H., Kroll, J., Seinfeld, J., and Wennberg, P.: Isoprene photooxidation: new insights into the production of acids and organic nitrates, Atmospheric Chemistry and Physics, 9, 1479–1501, 2009.

Rabitz, H. and Alis, O. F.: General foundations of high–dimensional model representations, Journal of Mathematical Chemistry, 25, 197–233, doi:10.1023/A:1019188517934, http://link.springer.com/article/10.1023/A%3A1019188517934, 1999.

Ren, X., Harder, H., Martinez, M., Lesher, R. L., Oliger, A., Simpas, J. B., Brune, W. H., Schwab, J. J., Demerjian, K. L., He, Y., Zhou, X., and Gao, H.: OH and HO2 Chemistry in the urban atmosphere of New York City, Atmospheric Environment, 37, 3639–3651, doi:10.1016/S1352-2310(03)00459-X, 2003.

Ren, X., Brune, W. H., Cantrell, C. A., Edwards, G. D., Shirley, T., Metcalf, A. R., and Lesher, R. L.: Hydroxyl and Peroxy Radical Chemistry in a Rural Area of Central Pennsylvania: Observations and Model Comparisons, J Atmos Chem, 52, 231–257, doi:10.1007/s10874-005-3651-7, http://link.springer.com/article/10.1007/s10874-005-3651-7, 2005.

Ren, X., van Duin, D., Cazorla, M., Chen, S., Mao, J., Zhang, L., Brune, W. H., Flynn, J. H., Grossberg, N., Lefer, B. L., Rappenglück, B., Wong, K. W., Tsai, C., Stutz, J., Dibb, J. E., Thomas Jobson, B., Luke, W. T., and Kelley, P.: Atmospheric oxidation chemistry and ozone production: Results from SHARP 2009 in Houston, Texas, Journal of Geophysical Research: Atmospheres, 118, 5770–5780, doi:10.1002/jgrd.50342, 2013.

Riedel, T. P., Wagner, N. L., Dub, W. P., Middlebrook, A. M., Young, C. J., Öztürk, F., Bahreini, R., VandenBoer, T. C., Wolfe, D. E., Williams, E. J., Roberts, J. M., Brown, S. S., and Thornton, J. A.: Chlorine activation within urban or power plant plumes: Vertically resolved ClNO2 and Cl2 measurements from a tall tower in a polluted continental setting, J. Geophys. Res. Atmos., 118, 8702–8715, doi:10.1002/jgrd.50637, http://onlinelibrary.wiley.com/doi/10.1002/jgrd.50637/abstract, 2013.

Riedel, T. P., Wolfe, G. M., Danas, K. T., Gilman, J. B., Kuster, W. C., Bon, D. M., Vlasenko, A., Li, S.-M., Williams, E. J., Lerner, B. M., Veres, P. R., Roberts, J. M., Holloway, J. S., Lefer, B., Brown, S. S., and Thornton, J. A.: An MCM modeling study of nitryl chloride (ClNO2) impacts on oxidation, ozone production and nitrogen oxide partitioning in polluted continental outflow, Atmos. Chem. Phys., 14, 3789–3800, doi:10.5194/acp-14-3789-2014, http://www.atmos-chem-phys.net/14/3789/2014/, 2014.

Roberts, J. M., Osthoff, H. D., Brown, S. S., Ravishankara, A. R., Coffman, D., Quinn, P., and Bates, T.: Laboratory studies of products of N2O5 uptake on Clâ containing substrates, Geophys. Res. Lett., 36, L20 808, doi:10.1029/2009GL040448, http://onlinelibrary.wiley.com/doi/10.1029/2009GL040448/abstract, 2009.

Rohrer, F., Bohn, B., Brauers, T., Brüning, D., Johnen, F.-J., Wahner, A., and Kleffmann, J.: Characterisation of the photolytic HONO-source in the atmosphere simulation chamber SAPHIR, Atmos. Chem. Phys., 5, 2189–2201, doi:10.5194/acp-5-2189-2005, 2005.

Rolph, G.: READY - Real-time Environmental Applications and Display sYstem, http://ready.arl.noaa.gov: Accessed 3 Jan. 2016., 2016.

Sander, S., Abbatt, J., Barker, J., Burkholder, J., Friedl, R., Golden, D., Huie, R., Kolb, C., Kurylo, M., Moortgat, G., Orkin, V., and Wine, P.: Chemical Kinetics and Photochemical Data for Use in Atmospheric Studies, Evaluation No. 17, JPL Publication 10-6, http://jpldataeval.jpl.nasa.gov, 2011.

Saunders, S. M., Jenkin, M. E., Derwent, R. G., and Pilling, M. J.: Protocol for the development of the Master Chemical Mechanism, MCM v3 (Part A): tropospheric degradation of non-aromatic volatile organic compounds, Atmospheric Chemistry and Physics, 3, 161–180, doi:10.5194/acp-3-161-2003, http://www.atmos-chem-phys.net/3/161/2003/, 2003.

Seinfeld, J. H. and Pandis, S. N.: Atmospheric chemistry and physics: from air pollution to climate change, John Wiley & Sons, 2012.

Sheehy, P., Volkamer, R., Molina, L., and Molina, M.: Oxidative capacity of the Mexico City atmosphere–Part 2: A RO x radical cycling perspective, Atmospheric Chemistry and Physics, 10, 6993–7008, 2010.

Shirley, T., Brune, W., Ren, X., Mao, J., Lesher, R., Cardenas, B., Volkamer, R., Molina, L., Molina, M. J., Lamb, B., et al.: Atmospheric oxidation in the Mexico City metropolitan area (MCMA) during April 2003, Atmospheric Chemistry and Physics, 6, 2753–2765, 2006.

Spencer, K., McCabe, D., Crounse, J., Olson, J., Crawford, J., Weinheimer, A., Knapp, D., Montzka, D., Cantrell, C., Hornbrook, R., et al.: Inferring ozone production in an urban atmosphere using measurements of peroxynitric acid, Atmospheric Chemistry and Physics, 9, 3697–3707, 2009.

Staikova, M., Donaldson, D., and Francisco, J. S.: Overtone-induced reactions on the HO2NO2 potential surface, The Journal of Physical Chemistry A, 106, 3023–3028, 2002.

Stein, A. F., Draxler, R. R., Rolph, G. D., Stunder, B. J. B., Cohen, M. D., and Ngan, F.: NOAA's HYSPLIT Atmospheric Transport and Dispersion Modeling System, Bull. Amer. Meteor. Soc., 96, 2059–2077, doi:10.1175/BAMS-D-14-00110.1, http://journals.ametsoc.org/doi/10.1175/BAMS-D-14-00110.1, 2015.

Stemmler, K., Ammann, M., Donders, C., Kleffmann, J., and George, C.: Photosensitized reduction of nitrogen dioxide on humic acid as a source of nitrous acid, Nature, 440, 195–198, 2006.

Stockwell, W. R., Kirchner, F., Kuhn, M., and Seefeld, S.: A new mechanism for regional atmospheric chemistry modeling, Journal of Geophysical Research: Atmospheres, 102, 25 847 – 25 879, doi:10.1029/97JD00849, 1997.

Thornton, J. A. and Abbatt, J. P. D.: N2O5 Reaction on Submicron Sea Salt Aerosol: Kinetics, Products, and the Effect of Surface Active Organics, J. Phys. Chem. A, 109, 10 004–10 012, doi:10.1021/jp054183t, http://dx.doi.org/10.1021/jp054183t, 2005.

Thornton, J. A., Wooldridge, P. J., Cohen, R. C., Martinez, M., Harder, H., Brune, W. H., Williams, E. J., Roberts, J. M., Fehsenfeld, F. C., Hall, S. R., Shetter, R. E., Wert, B. P., and Fried, A.: Ozone production rates as a function of NOx abundances and HOx production rates in the Nashville urban plume, Journal of Geophysical Research: Atmospheres, 107, 7–17, doi:10.1029/2001JD000932, 2002.

Thornton, J. A., Kercher, J. P., Riedel, T. P., Wagner, N. L., Cozic, J., Holloway, J. S., Dubé, W. P., Wolfe, G. M., Quinn, P. K., Middlebrook, A. M., Alexander, B., and Brown, S. S.: A large atomic chlorine source inferred from mid-continental reactive nitrogen chemistry, Nature, 464, 271–274, doi:10.1038/nature08905, http://www.nature.com/nature/journal/v464/n7286/full/nature08905.html, 2010.

Tonnesen, G. S. and Dennis, R. L.: Analysis of radical propagation efficiency to assess ozone sensitivity to hydrocarbons and NOx : 1. Local indicators of instantaneous odd oxygen production sensitivity, Journal of Geophysical Research: Atmospheres, 105, 9213–9225, doi:10.1029/1999JD900371, 2000.

Trainer, M., Parrish, D. D., Goldan, P. D., Roberts, J., and Fehsenfeld, F. C.: Review of observation-based analysis of the regional factors influencing ozone concentrations, Atmospheric Environment, 34, 2045–2061, doi:10.1016/S1352-2310(99)00459-8, http://www.sciencedirect.com/science/article/pii/S1352231099004598, 2000.

Treadaway, V.: Measurement of Formic and Acetic Acid in Air by Chemical Ionization Mass Spectroscopy: Airborne Method Development, Master's thesis, University of Rhode Island, http://digitalcommons.uri.edu/theses/603, Paper 603, 2015.

Trebs, I., Bohn, B., Ammann, C., Rummel, U., Blumthaler, M., Königstedt, R., Meixner, F. X., Fan, S., and Andreae, M. O.: Relationship between the NO_2 photolysis frequency and the solar global irradiance, Atmospheric Measurement Techniques, 2, 725–739, doi:10.5194/amt-2-725-2009, http://www.atmos-meas-tech.net/2/725/2009/, 2009.

US EPA: Laboratory study to explore potential interferences to air quality monitors, Govt. Doc. EP 4.52:2002006990, Office of Air Quality Planning and Standards, Research Triangle Park, NC Accessed online: 2014-01-04, 1999.

US EPA: Integrated Science Assessment of Ozone and Related Photochemical Oxidants(Final Report), Govt. Doc. EPA/600/R - 10/076F, Office of Research and Development, National Center for Environmental Assessment- RTP Division, Research Triangle Park, NC, 2013.

US EPA: Ozone Trends, https://www.epa.gov/air-trends/ozone-trends, Accessed 22 April 2016., 2016a.

US EPA: Ozone NAAQS | US EPA, https://www3.epa.gov/ttn/naaqs/standards/ozone/s_o3_index.html, 2016b.

Volkamer, R., Sheehy, P., Molina, L., and Molina, M.: Oxidative capacity of the Mexico City atmosphere–Part 1: A radical source perspective, Atmospheric Chemistry and Physics, 10, 6969–6991, 2010.

Wagner, N. L., Riedel, T. P., Young, C. J., Bahreini, R., Brock, C. A., Dubé, W. P., Kim, S., Middlebrook, A. M., Öztürk, F., Roberts, J. M., Russo, R., Sive, B., Swarthout, R., Thornton, J. A., VandenBoer, T. C., Zhou, Y., and Brown, S. S.: N2O5 uptake coefficients and nocturnal NO2 removal rates determined from ambient wintertime measurements, J. Geophys. Res. Atmos., 118, 9331–9350, doi:10.1002/jgrd.50653, http://onlinelibrary.wiley.com/doi/10.1002/jgrd.50653/abstract, 2013.

Wainman, T., Weschler, C. J., Lioy, P. J., and Zhang, J.: Effects of surface type and relative humidity on the production and concentration of nitrous acid in a model indoor environment, Environmental Science & Technology, 35, 2201–2206, PMID: 11414019, 2001.

Weibring, P., Richter, D., Fried, A., Walega, J., and Dyroff, C.: Ultra-high-precision mid-IR spectrometer II: system description and spectroscopic performance, Applied Physics B, 85, 207–218, 2006.

Weibring, P., Richter, D., Walega, J. G., and Fried, A.: First demonstration of a high performance difference frequency spectrometer on airborne platforms, Optics Express, 15, 13 476–13 495, 2007.

Wilson, K. L. and Birks, J. W.: Mechanism and elimination of a water vapor interference in the measurement of ozone by UV absorbance, Environmental Science & Technology, 40, 6361–6367, PMID: 17120566, 2006.

Wolfe, G. M., Thornton, J. A., Bouvier-Brown, N. C., Goldstein, A. H., Park, J.-H., McKay, M., Matross, D. M., Mao, J., Brune, W. H., LaFranchi, B. W., Browne, E. C., Min, K.-E., Wooldridge, P. J., Cohen, R. C., Crounse, J. D., Faloona, I. C., Gilman, J. B., Kuster, W. C., de Gouw, J. A., Huisman, A., and Keutsch, F. N.: The Chemistry of Atmosphere-Forest Exchange (CAFE) Model Part 2: Application to BEARPEX-2007 observations, Atmos. Chem. Phys., 11, 1269–1294, doi:10.5194/acp-11-1269-2011, http://www.atmos-chem-phys.net/11/1269/2011/, 2011.

Xue, L. K., Saunders, S. M., Wang, T., Gao, R., Wang, X. F., Zhang, Q. Z., and Wang, W. X.: Development of a chlorine chemistry module for the Master Chemical Mechanism, Geosci. Model Dev., 8, 3151–3162, doi:10.5194/gmd-8-3151-2015, http://www.geosci-model-dev.net/8/3151/2015/, 2015.

Zetzsch, C. and Behnke, W.: Heterogeneous Photochemical Sources of Atomic Cl in the Troposphere, Berichte der Bunsengesellschaft physikalische Chemie, 96, 488–493, doi:10.1002/bbpc.19920960351, http://onlinelibrary.wiley.com/doi/10.1002/bbpc.19920960351/abstract, 1992.

Zheng, W., Flocke, F. M., Tyndall, G. S., Swanson, A., Orlando, J. J., Roberts, J. M., Huey, L. G., and Tanner, D. J.: Characterization of a thermal decomposition chemical ionization mass spectrometer for the measurement of peroxy acyl nitrates (PANs) in the atmosphere, Atmospheric Chemistry and Physics, 11, 6529–6547, doi:10.5194/acp-11-6529-2011, http://www.atmos-chem-phys.net/11/6529/2011/, 2011.

Atmos. Chem. Phys. Discuss., doi:10.5194/acp-2016-1089, 2017
Manuscript under review for journal Atmos. Chem. Phys.
Published: 4 January 2017

Atmospheric Chemistry and Physics Discussions

Table 1. Measured parameters input into the RACM2 and MCMv331. Inorganic chemical species measurement time resolution is 1 min. Aircraft chemical species were measured every 1 s. Evacuated whole-air canister VOC point measurements were interpolated to 1-h medians as described in Section 2.2. All measured constraints were either averaged or interpolated to 10 min for model runs.

Number	Model input	Method[b]	Uncertainty (%)	Institution
8	**Inorganics**			
	O_3	CL	10	EPA
	SO_2	UV Fluorescence	10	
	NO_2, NO	CES/CAPS, CL	10	
	CO, CO_2, CH_4	WACs/GC/GC-MS (Colman et al., 2001)	≤ 5	UCI
	HNO_3	TD-LIF (Day et al., 2002)	25	UC Berkeley[a]
58	**Organic Species**			
42	C_2-C_{10} *NMHCs*, *organic nitrates*: ethane, ethene, acetylene, propane, propene, i-butane, n-butane, i-pentane, n-pentane, isoprene, n-hexane, n-heptane, n-octane, 2,3-dimethylbutane, 2-methylpentane, 3-methylpentane, 2,4-dimethylpentne, 2,2,4-trimethylpentane,cyclopentane,methylcyclopentane, cyclohexane, methylcyclohexane, benzene, toluene, ethylbenzene, m,p-xylene, o-xylene, 2-ethyltoluene, 3-ethyltoluene, 4-ethyltoluene, 1,3,5-trimethylbenzene, 1,2,4-trimethylbenzene, 1,2,3-trimethylbenzene, α-pinene, β-pinene, methyl nitrate, ethyl nitrate, i-propylnitrate, 2-butylnitrate, 2-pentylnitrate, 3-pentylnitrate, 2-methyl-2-butylnitrate	WACs/GC/GC-MS (Colman et al., 2001)	3-100	UCI
	NMHCs[a]: methyl ethyl ketone, methanol, methyl vinyl ketone, methacrolein, acetic acid acetaldehyde, acetone	PTR-ToF-MS (Müller et al., 2014)	10	U. Innsbruck
	formaldehyde	DFGAS (Weibring et al., 2006, 2007)	5	CU-INSTAAR
	peroxy acetyl nitrate, peroxy propyl nitrate	PAN-CIMS (Zheng et al., 2011)	13	NCAR
	hydrogen peroxide, formic acid, acetic acid	PCIMS (Treadaway, 2015)	30	URI
	ethanol, d-limonene/3-carene, camphene	TOGA (Apel et al., 2003)	30	NCAR

[a] Denotes aircraft measurements
[b] CL, chemiluminescence; CES, cavity enhanced spectroscopy; CAPS, cavity attenuated phase shift spectrometer; WAC, whole-air canister; GC, gas chromatography; GC-MS, gas chromatography mass spectrometer; TD-LIF, thermal dissociation laser-induced fluorescence; PTR-ToF-MS, proton transfer reaction time-of-flight mass spectrometer; DFGAS, difference frequency generation absorption spectrometer; CIMS, chemical ionization mass spectrometer ('PAN', peroxyacyl nitrate; 'P', peroxide); TOGA, trace organic gas analyzer.

Atmos. Chem. Phys. Discuss., doi:10.5194/acp-2016-1089, 2017
Manuscript under review for journal Atmos. Chem. Phys.
Published: 4 January 2017

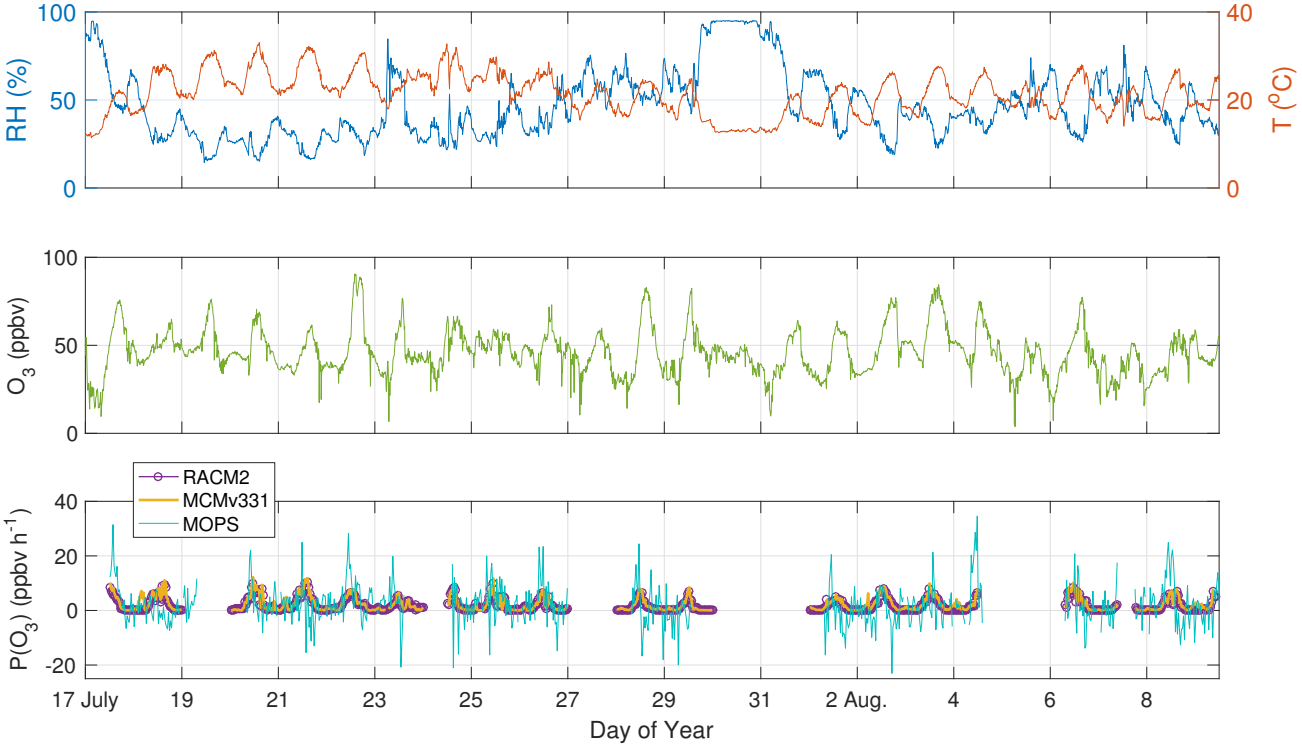

Figure 1. Top: Full-campaign 10-minute temperature and relative humidity in Golden, CO. The “warm" period is defined as days before 27 July 2014. Middle: Full-campaign 10-min O_3 mixing ratios for 17 July to 10 August 2014. Bottom: $P(O_3)$ measured by the MOPS and modeled from the RACM2 and MCMv331 for the same time period. Measured to modeled comparisons are shown for days with available MOPS measurements and have a 30-min time resolution.

Atmos. Chem. Phys. Discuss., doi:10.5194/acp-2016-1089, 2017
Manuscript under review for journal Atmos. Chem. Phys.
Published: 4 January 2017

Atmospheric Chemistry and Physics Discussions

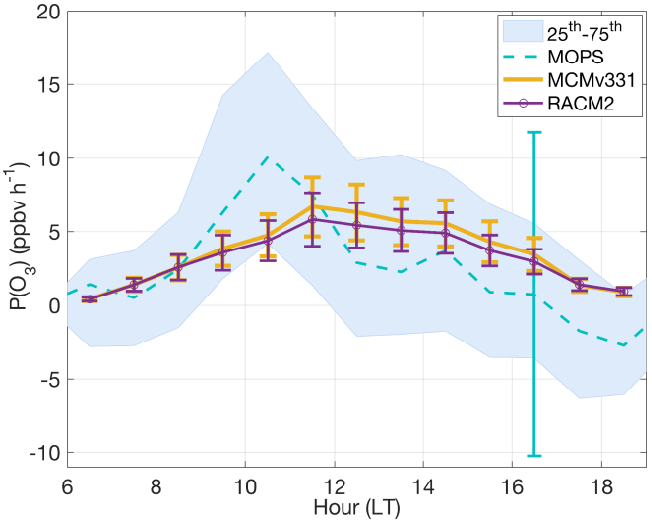

Figure 2. Full-campaign median hourly $P(O_3)$ measured by the MOPS, and modeled by the RACM2 and MCMv331 for daylight hours between 0600-1800 local time. Diel values shown are shown only for days with MOPS measurements. The MOPS absolute standard deviation (1σ) is shown for 1600 and the RACM2 and MCMv331 relative error bars are shown at the 1σ confidence level. Shown as a shaded area is the MOPS 25th and 75th percentiles.

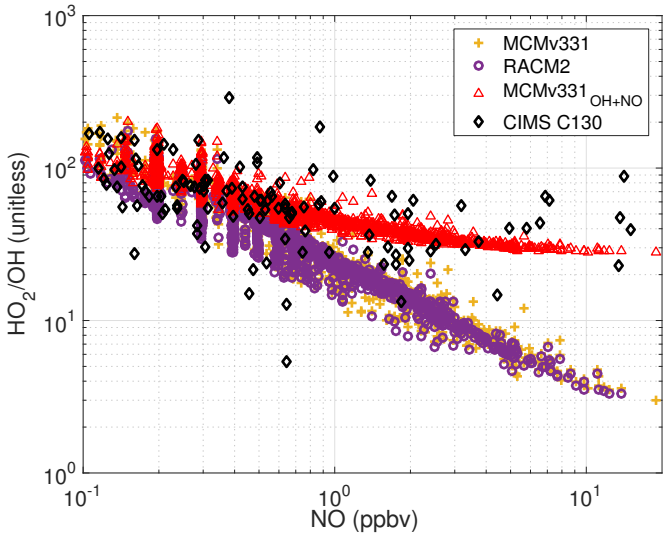

Figure 3. C-130 aircraft CIMS HO_2/OH ratio as a function of aircraft NO (chemiluminescence, 20 pptv $\pm$ 10%, 1σ uncertainty) around the vicinity of Golden, CO, and modeled HO_2/OH ratio using constrained NO measured in Golden, CO. Aircraft measurements used are limited to the first 1 km in the boundary layer, and a well-mixed boundary layer is assumed for the HO_x measurements. MCMv331 model results are shown for the OH + NO + O_2 reaction to yield HO_2 + NO_2 using the kinetic rate coefficient of (9-15)x10^{-11}cm^{3}molecule^{-1}s^{-1} discussed in Section 3.3.4.

Atmos. Chem. Phys. Discuss., doi:10.5194/acp-2016-1089, 2017
Manuscript under review for journal Atmos. Chem. Phys.
Published: 4 January 2017

Atmospheric Chemistry and Physics Discussions

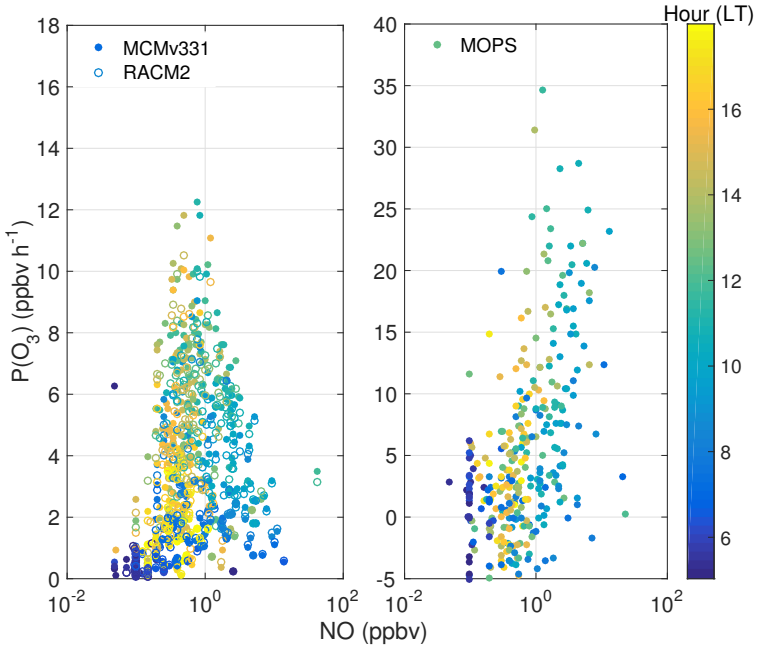

Figure 4. RACM2, MCMv331 (left), and MOPS (right) 30-minute $P(O_3)$ as a function NO for total campaign data. Points are colored by hour of day.

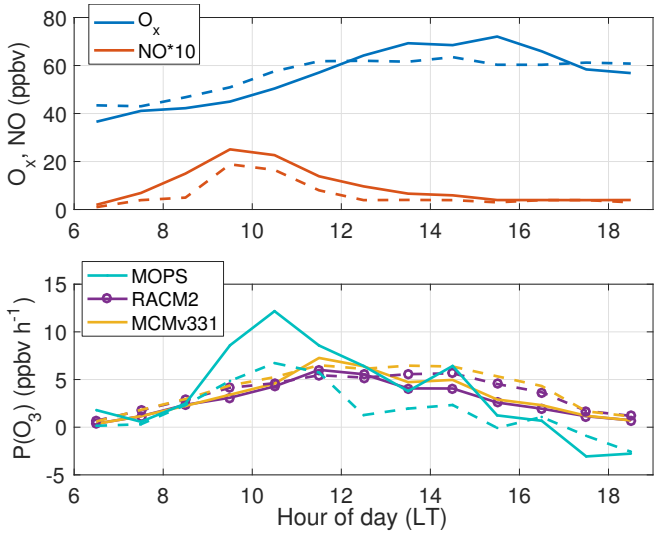

Figure 5. Top: O_x (O_3 + NO_2) and NO mixing ratios for Denver plume (solid) versus all other days (dashed) from 17 July - 10 August 2014 in Golden, CO. Bottom: Median measured and modeled $P(O_3)$ for Denver plume (solid) and non-Denver plume (dashed) days between 0600-1800 LT.